Available online at www.sciencedirect.com
ScienceDirect
Nuclear Physics B 807 [FS] (2009) 424–454
NUCLEAR PHYSICS B
www.elsevier.com/locate/nuclphysb

# Tethered Monte Carlo: Computing the effective potential without critical slowing down

L.A. Fernandez [a,b], V. Martin-Mayor [a,b], D. Yllanes [a,b,*]

[a] *Departamento de Física Teórica I, Facultad de CC. Físicas, Universidad Complutense de Madrid, 28040 Madrid, Spain*

[b] *Instituto de Biocomputación y Física, de Sistemas Complejos (BIFI), Zaragoza, Spain*

Received 6 June 2008; accepted 11 July 2008

Available online 18 July 2008

**Abstract**

We present Tethered Monte Carlo, a simple, general purpose method of computing the effective potential of the order parameter (Helmholtz free energy). This formalism is based on a new statistical ensemble, closely related to the micromagnetic one, but with an extended configuration space (through Creutz-like demons). Canonical averages for arbitrary values of the external magnetic field are computed without additional simulations. The method is put to work in the two-dimensional Ising model, where the existence of exact results enables us to perform high precision checks. A rather peculiar feature of our implementation, which employs a local Metropolis algorithm, is the total absence, within errors, of critical slowing down for magnetic observables. Indeed, high accuracy results are presented for lattices as large as $L = 1024$.


*PACS:* 75.40.Mg; 05.10.Ln; 05.50.+g

*Keywords:* Monte Carlo; Critical phenomena; Phase transitions; Ising model

## 1. Introduction

There exists a very profound relation between quantum field theory and statistical mechanics, through the theory of critical phenomena [1–3]. In the examination of these phenomena Monte

* Corresponding author.
*E-mail address:* yllanes@lattice.fis.ucm.es (D. Yllanes).

0550-3213/$ – see front matter 
doi:10.1016/j.nuclphysb.2008.07.009

Carlo simulations [4] are an indispensable tool, because of their exceedingly broad range of applicability. Indeed, Monte Carlo simulations not only succeed where an analytical treatment would be impossible or impractical, but they are many times the only numerical method capable of tackling the problem at hand.

There are some difficulties, though, among which we can mention critical slowing down [2,5]. For traditional Monte Carlo formalisms the correlation times (roughly, the number of intermediate steps so that two measurements can be considered independent) grow as $L^z$ at the critical point (with $z \approx 2$). A great step towards the solution of this problem was taken in the late 1980s, with the development of the first cluster methods [6], capable of achieving $z < 1$. This prompted a large amount of work on more sophisticated cluster algorithms, which continues today [7].

Unfortunately, cluster methods are highly specific and we do not know how to efficiently implement them for physical problems as important as lattice gauge theories [8], with or without dynamic fermions; structural glasses [9]; spin glasses [10]; protein folding [11] and a long etcetera. Even in their favourite playground, ferromagnetic systems, cluster methods lose most of their power in the presence of a magnetic field. The simplest example is the $D = 2$ Ising model, whose exact solution without a magnetic field is known since 1944 [12], but whose behaviour with a magnetic perturbation is still an active research topic [13,14]. It is interesting to notice that the current numerical methods of choice rely on transfer matrix techniques [15] and not on Monte Carlo simulations.

Here we present the Tethered Monte Carlo (TMC) method, a completely unspecific strategy, appliable to many problems with or without an external field. The main goal of this approach is constructing the effective potential of the order parameter (perhaps more commonly named Helmholtz free energy in a statistical mechanics context).

In order to define this Monte Carlo method, we shall introduce a new statistical ensemble, where the magnetic field and the order parameter exchange their roles with respect to the canonical ensemble.[1] This new framework has some interesting features of its own. For example, when working with a ferromagnetic system it provides a very clean definition of the broken symmetry phase for a finite lattice.

In the ferromagnetic setting the tethered ensemble is related to the micromagnetical one, where both the temperature $\beta$ and the magnetisation density $m$ are kept fixed. The difference is that here we couple $m$ to a Gaussian 'magnetostat'. This yields a new variable $\hat{m}$ which, unlike $m$, is continuous even for finite lattices. The magnetic field is obtained from a fluctuation–dissipation formalism. We can then work at constant $\hat{m}$, where the real magnetisation is almost fixed, but has some leeway (hence the name *tethered*). We then combine the mean values at constant $\hat{m}$ of the magnetic field to construct the effective potential $\Omega_N(\hat{m})$, whose exponential gives the canonical probability density function (pdf) of $\hat{m}$. Using this pdf and the mean values of the different physical observables as a function of $\hat{m}$ we can recover the canonical results.

The tethered ensemble is not only a fancy theoretical construct, but also the basis for a practical simulation method. It is straightforward to implement it with, for example, the well known local Metropolis [16] update algorithm. We can thus run simulations at constant $\hat{m}$ and then combine them to obtain the canonical averages with very high precision. It would be also possible to search for a cluster algorithm compatible with the tethered formalism, but we shall not investigate this issue here.

[1] In the canonical ensemble the magnetic field is an external parameter and the order parameter an observable, while their tethered equivalents have the reversed roles.

One surprising feature of this Metropolis implementation is that we can find no traces of critical slowing down, within our errors, for all functions of $m$. Other quantities, such as the energy, exhibit the $z \approx 2$ behaviour typical of local algorithms. Another interesting point about this method is that, for a given temperature, $\Omega_N(\hat{m})$ has all the information about the system so we can, for example, extract the canonical results at any value of the applied magnetic field $h$ without recomputing the tethered mean values (i.e., without any new simulations, see Section 7).

The TMC method is an extension of the strategy introduced in [17]: there the configuration space was extended to work in a microcanonical ensemble, with entropy as the main physical variable. The motivation in [17] was handling first order transitions without the need for tunnelling between two coexisting phases. The microcanonical method was first applied in [17] to a pure system and was later, in [18], instrumental in simulating a phase transition which remained first order in the presence of quenched disorder. Both the TMC and microcanonical methods have deep links to Creutz's microcanonical demon [19]. The main differences are: (i) we have as many demons as spins, (ii) our demons are continuous variables and (iii) we explicitly integrate out the demons, finding a tractable effective Hamiltonian.

The effective potential can also be computed using multicanonical methods [20], sometimes named multimagnetical [21], or with the Wang–Landau algorithm [22]. A major difference is that TMC does not require a random walk in magnetisation space (as with multimagnetical methods) or in the energy–magnetisation plane (as in Wang–Landau). Indeed, we have worked with as many as $10^6$ spins, while $10^3$ spins is a typical limit for Wang–Landau computations [23]. On the other hand, standard micromagnetical methods [24] do not render the effective potential.

In this paper we give a detailed exposition of the TMC method and demonstrate it in the standard benchmark of the two-dimensional Ising model. Our motivation for this choice is twofold. On the one hand, since Onsager's solution [12] many other exact results have been obtained (for a review see [25] and references therein), which will help us check that our answers are correct. This model is also the ideal scenario for cluster methods, so even for those observables whose exact value is unknown we can check our results to a high degree of accuracy against a cluster simulation. On the other hand, the Ising model is sufficiently well known and simple that we may concentrate on examining the details of the method with a minimum of nonessential discussion. We purpose to show that TMC is capable of rendering very precise results and try to convince the reader that it will still be efficient for harder problems.

The rest of the paper is organised as follows:

- In Section 2 we describe our statistical ensemble and its relationship with the standard canonical ensemble and properly define the effective potential. In Section 3 we explain in detail how to set up a simulation using the TMC method. We then examine our own simulations for the Ising model. In Section 4 we show that our algorithm presents no measurable traces of critical slowing down for the magnetic field.
- We have carried out simulations at the critical point and in both the ferromagnetic and paramagnetic phases, with and without a magnetic field. Our results at the critical temperature and zero magnetic field are presented in Section 5 and compared both with the exact results at finite $L$ given by [26] and with high precision Swendsen–Wang simulations (Section 5.2). In Section 5.3 we shall compute very accurately the magnetisation critical exponent in a fairly unusual way, made easy by TMC. In Section 6 we check the performance of the method in the scaling paramagnetic region. Our chosen test has been the computation of the first renormalised coupling constants.

- The magnetic field $h$ is introduced in Section 7, where we obtain several observables as a function of $h$ and check our results with FSS arguments and by recomputing the nonlinear susceptibilities with a finite differences formula. Section 8 demonstrates the enhanced effectivity of the method in the ferromagnetic regime, where we work with and without an external field.
- Finally, in Section 9 we present our conclusions and outlook. We give some technical details of our numerical implementation in Appendix A.

## 2. The statistical ensemble

### 2.1. The model and the canonical observables

We shall work with the $D = 2$ Ising model, defined by the following partition function,

$$Z = \sum_{\{\sigma_{\boldsymbol{x}}\}} \mathrm{e}^{\beta \sum_{\langle \boldsymbol{x},\boldsymbol{y}\rangle} \sigma_{\boldsymbol{x}}\sigma_{\boldsymbol{y}} + h \sum_{\boldsymbol{x}} \sigma_{\boldsymbol{x}}}, \quad \sigma_{\boldsymbol{x}} = \pm 1, \tag{1}$$

where $h$ is the applied magnetic field, $\boldsymbol{x} = (x_1, x_2)$ and $\langle \boldsymbol{x}, \boldsymbol{y}\rangle$ stands for lattice nearest neighbours. We shall always consider square lattices with $N = L^2$ spins and periodic boundary conditions. The infinite volume model has a second order phase transition at a critical (inverse) temperature $\beta_{\mathrm{c}}$ given by

$$\beta_{\mathrm{c}} = \frac{\log(1+\sqrt{2})}{2} = 0.440686793509771\ldots \tag{2}$$

The simplest observables are the energy and magnetisation,[2]

$$U = Nu = -\sum_{\langle \boldsymbol{x},\boldsymbol{y}\rangle} \sigma_{\boldsymbol{x}}\sigma_{\boldsymbol{y}}, \tag{3}$$

$$M = Nm = \sum_{\boldsymbol{x}} \sigma_{\boldsymbol{x}}. \tag{4}$$

In the canonical ensemble we are concerned with thermal averages, which we shall denote by $\langle\,\cdot\,\rangle_\beta$:

$$U_\beta = Nu_\beta = \langle U\rangle_\beta, \tag{5}$$

$$M_\beta = Nm_\beta = \langle M\rangle_\beta. \tag{6}$$

The specific heat and magnetic susceptibility are

$$C = N\big[\langle u^2\rangle_\beta - \langle u\rangle_\beta^2\big], \tag{7}$$

$$\chi_2 = N\big[\langle m^2\rangle_\beta - \langle m\rangle_\beta^2\big]. \tag{8}$$

[2] We shall use sans-serif italics for random variables (i.e., functions of the spins) and serif italics for real numbers (e.g. expectation values or arguments of the probability density functions). This will help emphasise which quantities are kept fixed and which can change. We shall also use lowercase letters for intensive quantities and uppercase letters for extensive quantities.

The latter quantity can be seen as the zero momentum component of the two point correlation function:

$$G_2(\boldsymbol{k}) = \frac{1}{N}\sum_{\boldsymbol{x}} \langle \sigma_{\boldsymbol{x}}\sigma_{\boldsymbol{0}}\rangle_\beta \mathrm{e}^{\mathrm{i}\boldsymbol{k}\cdot\boldsymbol{x}}. \tag{9}$$

If we consider the asymptotic behaviour of the propagator in position space we arrive at the concept of *correlation length*,

$$\xi_{\exp} = \lim_{|\boldsymbol{x}|\to\infty} \frac{-|\boldsymbol{x}|}{\log \tilde{G}_2(\boldsymbol{x})}. \tag{10}$$

This quantity is not easily measurable in our finite lattices, so we would like to have a better statistically behaved definition that could also be interpreted as a correlation length. In momentum space and in the limit $\xi_{\exp}|\boldsymbol{k}| \to 0$, the propagator is well described by the free field form [1,2]

$$G_2(\boldsymbol{k}) \simeq \frac{A}{\xi^{-2} + 4\sum_{i=1,2}\sin^2 k_i/2}. \tag{11}$$

($A$ is a constant.) If we combine this formula at zero momentum and at the smallest nonzero momentum $\boldsymbol{k}_1$ we obtain

$$\xi_1 = \frac{1}{2\sin(\pi/L)}\left[\frac{G_2(0)}{G_2(\boldsymbol{k}_1)} - 1\right]^{1/2}, \tag{12}$$

with $G_2(\boldsymbol{k}_1)$ averaged over $\boldsymbol{k}_1 = (2\pi/L, 0), (0, 2\pi/L)$. This definition [27] has proven to be extremely useful in Finite Size Scaling studies [28,29].

Eq. (12) does not work in the broken symmetry phase or with an applied magnetic field, because then $G_2(\boldsymbol{k})$ becomes singular at $\boldsymbol{k} = 0$. We can still use (11) for $\boldsymbol{k} \neq 0$ and consider a second definition of the correlation length, now combining the two smallest nonzero momenta,

$$\xi_2 = \frac{1}{2\sin(\pi/L)}\left[\frac{G_2(\boldsymbol{k}_1) - G_2(\boldsymbol{k}_2)}{2G_2(\boldsymbol{k}_2) - G_2(\boldsymbol{k}_1)}\right]^{1/2}, \tag{13}$$

with $G_2(\boldsymbol{k}_2)$ averaged over $\boldsymbol{k}_2 = (2\pi/L, \pm 2\pi/L)$ and $G_2(\boldsymbol{k}_1)$ as in definition (12). The two definitions, $\xi_1$ and $\xi_2$, coincide for $\beta < \beta_c$, but only in thermodynamic limit.

Other observables are the Binder ratio

$$B = \frac{\langle M^4\rangle_\beta}{\langle M^2\rangle_\beta^2} \tag{14}$$

and the $2n$ point correlation functions at zero momentum,

$$\chi_{2n} = \frac{1}{N}\frac{\partial^{2n}\log(Z)}{(\partial h)^{2n}}. \tag{15}$$

Notice that these are just the cumulants of the magnetisation. In the low temperature phase we should also consider odd derivatives.

### 2.2. The tethered ensemble

Let us consider the Ising model without an external field ($h = 0$). We can define a probability density function (pdf) for $M$, which will be a sum of $N + 1$ Dirac deltas,

$$p_1(m) = \frac{1}{Z}\sum_{\{\sigma_x\}} \exp[-\beta U]\delta\Big(m - \sum_i \sigma_i/N\Big), \quad Z = \sum_{\{\sigma_x\}} \exp[-\beta U]. \tag{16}$$

In the thermodynamic limit $p_1(m)$ is non-vanishing for all $m$ in $[-1, 1]$. We would like to have a new quantity that would be continuous even for finite lattices. As a first step, we extend our configuration space with $N$ Gaussian demons[3]:

$$Z = \int_{-\infty}^{\infty} \prod_{i=1}^{N} \mathrm{d}\eta_i \sum_{\{\sigma_x\}} \exp\Big[-\beta U - \sum_i \eta_i^2/2\Big], \qquad R = Nr = \sum_i \eta_i^2/2, \tag{17}$$

$$p_2(r) = \frac{1}{Z}\int_{-\infty}^{\infty} \prod_{i=1}^{N} \mathrm{d}\eta_i \sum_{\{\sigma_x\}} \exp\Big[-\beta U - \sum_i \eta_i^2/2\Big]\delta\Big(r - \sum_i \eta_i^2/(2N)\Big). \tag{18}$$

Notice that in the canonical formalism the demons are a thermal bath decoupled from the spins because the spin contribution in (18) cancels out. By virtue of the Central Limit Theorem, the pdf for $r$ approaches a Gaussian of mean $1/2$ and variance $(2N)^{-1}$ in the large $N$ limit.

Now we introduce $\hat{M} = N\hat{m} = M + R$. The new variable $\hat{m}$ is continuous and its pdf is simply the convolution of those of $m$ and $r$ (as these are statistically independent):

$$p(\hat{m}) = \int_{-1}^{1} \mathrm{d}m \int_{0}^{\infty} \mathrm{d}r\; p_1(m)\, p_2(r)\delta(\hat{m} - m - r). \tag{19}$$

Notice that $\hat{M} \geqslant M$ and that $p(\hat{m})$ is essentially a smoothed version of $p_1(\hat{m} - 1/2)$. Finally, we introduce what will be our basic physical quantity, the *effective potential* $\Omega_N(\hat{m}, \beta)$,

$$p(\hat{m}) = \exp\big[N\Omega_N(\hat{m}, \beta)\big]. \tag{20}$$

The effective potential has all the information about the system at inverse temperature $\beta$, including what would happen if it were immersed in an external magnetic field.

Our next step is constructing the statistical ensemble and its relationship with the canonical one. In order to do this we represent $\Omega_N(\hat{m}, \beta)$ as a functional integral and integrate out the demons,

$$\begin{aligned} \mathrm{e}^{N\Omega_N(\hat{m},\beta)} &= \frac{1}{Z}\int_{-\infty}^{\infty} \prod_{i=1}^{N} \mathrm{d}\eta_i \sum_{\{\sigma_x\}} \mathrm{e}^{-\beta U - \sum_i \eta_i^2/2}\delta\Big(\hat{m} - m - \sum_i \eta_i^2/(2N)\Big) \\ &= \frac{1}{Z}\int_{-\infty}^{\infty} \prod_{i=1}^{N} \mathrm{d}\eta_i \sum_{\{\sigma_x\}} \mathrm{e}^{-\beta U + M - N\hat{m}}\delta\Big(\hat{m} - m - \sum_i \eta_i^2/(2N)\Big) \end{aligned}$$

[3] This is not the only possible choice. In fact, we have also experimented with Poissonian demons, better suited to a possible future implementation of this method in dedicated computers with specific hardware [30]. The results (both in simulation time and accuracy of the final values) were virtually identical.

$$= \frac{1}{Z}\sum_{\{\sigma_x\}} \mathrm{e}^{-\beta U + M - N\hat{m}}(\hat{m}-m)^{(N-2)/2}\frac{(2\pi N)^{N/2}\theta(\hat{m}-m)}{\Gamma(N/2)}. \tag{21}$$

The condition $\hat{m} \geqslant m$ is explicitly enforced by the Heaviside step function $\theta$. Notice as well that we have constructed the effective potential from the starting point of a canonical ensemble. It would be elementary to retrace our steps for a microcanonical $\Omega_N$ (we would just have to change the exponential of the energy in the previous equations to the appropriate microcanonical weight, see [17]).

We want to develop a statistical ensemble based on the effective potential (i.e. to define average values). To do this we differentiate $\Omega_N$,

$$\frac{\partial \Omega_N(\hat{m},\beta)}{\partial \hat{m}} = \frac{\sum_{\{\sigma_x\}}(-1+\frac{N-2}{2N(\hat{m}-m)})\omega(\beta,\hat{m},N;\{\sigma_x\})}{\sum_{\{\sigma_x\}}\omega(\beta,\hat{m},N;\{\sigma_x\})}, \tag{22}$$

where

$$\omega\big(\beta,\hat{m},N;\{\sigma_x\}\big) = \mathrm{e}^{-\beta U + M - N\hat{m}}(\hat{m}-m)^{(N-2)/2}\theta(\hat{m}-m). \tag{23}$$

Eqs. (22) and (23) suggest a new ensemble where the probability of a given configuration $\{\sigma_x\}$ is proportional to $\omega(\beta,\hat{m},N;\{\sigma_n\})$. Therefore, we can define the *tethered mean value* $\langle\cdot\rangle_{\hat{m},\beta}$ for an arbitrary observable $O$ by

$$\langle O\rangle_{\hat{m},\beta} = \frac{\sum_{\{\sigma_x\}} O(\hat{m};\{\sigma_x\})\omega(\beta,\hat{m},N;\{\sigma_x\})}{\sum_{\{\sigma_x\}}\omega(\beta,\hat{m},N;\{\sigma_x\})}. \tag{24}$$

Now we define the tethered magnetic field as

$$\hat{h}\big(\hat{m};\{\sigma_x\}\big) = -1 + \frac{N/2-1}{\hat{M}-M} \tag{25}$$

and notice from (22) and (24) that

$$\langle\hat{h}\rangle_{\hat{m},\beta} = \frac{\partial\Omega_N(\hat{m},\beta)}{\partial\hat{m}}. \tag{26}$$

The duality between the roles of $\hat{h}$ and $m$ in the canonical and tethered ensembles is best illustrated from the tethered fluctuation–dissipation formula:

$$\frac{\partial\langle O\rangle_{\hat{m},\beta}}{\partial\hat{m}} = \left\langle\frac{\partial O}{\partial\hat{m}}\right\rangle_{\hat{m},\beta} + N\big[\langle O\hat{h}\rangle_{\hat{m},\beta} - \langle O\rangle_{\hat{m},\beta}\langle\hat{h}\rangle_{\hat{m},\beta}\big]. \tag{27}$$

The simulation strategy is then clear: we compute the tethered averages of $\hat{h}$ and whichever observables we need for a reasonable number of values of $\hat{m}$ (we shall discuss what we mean by 'reasonable' in the next section). The effective potential cannot be measured directly, but we do have its derivative $\langle\hat{h}\rangle_{\hat{m},\beta}$. Integrating $\langle\hat{h}\rangle_{\hat{m},\beta}$ and requiring that the probability $p(\hat{m})$ be normalised we can obtain $\Omega_N(\hat{m},\beta)$ unambiguously.

Once we have the effective potential, we can recover the canonical averages with the following formula:

$$\langle O\rangle_\beta = \int \mathrm{d}\hat{m}\,\langle O\rangle_{\hat{m},\beta}\mathrm{e}^{N\Omega(\hat{m},\beta)}. \tag{28}$$

Thus far, we have defined the ensemble in the absence of an external magnetic field $h$, but we can include it very easily. Indeed, we just have to notice that an applied field introduces a shift in the

origin of $\hat{h}$. The computation of canonical averages with an external field is then straightforward, using the same tethered mean values we had for $h = 0$:

$$\langle O\rangle_\beta(h) = \frac{\int \mathrm{d}\hat{m}\, \mathrm{e}^{N[\Omega_N(\hat{m},\beta)+h\hat{m}]}\langle O\rangle_{\hat{m},\beta}}{\int \mathrm{d}\hat{m}\, \mathrm{e}^{N[\Omega_N(\hat{m},\beta)+h\hat{m}]}}. \tag{29}$$

The denominator is necessary because now the shifted effective potential is not normalised.

## 3. Description of the simulations

The basic steps in a TMC simulation, which we shall discuss later, are the following.

1. Select an appropriate sampling for $\hat{M}$ remembering that, essentially, $\hat{M} \simeq M + N/2$. We shall discuss the choice of the $\hat{m}$ grid in Section 3.1. Naturally, we must restrict ourselves to a finite simulation range, $[\hat{m}_{\min}, \hat{m}_{\max}]$, which introduces an (exponentially small) cutoff error.
2. Run independent simulations for each $\hat{m}$, measuring the tethered averages of $\hat{h}$ and the other relevant observables.
3. The mean values $\langle O\rangle_{\hat{m},\beta}$ are smooth functions of $\hat{m}$, so they can be interpolated safely. We use cubic splines [31], but other methods may also work. Appendix A has some technical details about this and other points of our implementation.
4. Integrate $\langle \hat{h}\rangle_{\hat{m},\beta}$ for the whole range of $\hat{m}$. We use an average of the integral in both directions to reduce the systematic error:

$$I_N(\hat{m},\beta) = \frac{1}{2}\left( \int_{\hat{m}_{\min}}^{\hat{m}} \mathrm{d}\hat{m}'\, \langle \hat{h}\rangle_{\hat{m}',\beta} - \int_{\hat{m}}^{\hat{m}_{\max}} \mathrm{d}\hat{m}'\, \langle \hat{h}\rangle_{\hat{m}',\beta} \right). \tag{30}$$

   This defines $\Omega_N(\hat{m},\beta)$ up to an additive constant. Notice that this is not the same as forcing $\Omega_N(\hat{m},\beta)$ to be symmetric (which it cannot be, since $\hat{m}$ has a finite lower bound but extends to infinity).
5. Normalise the pdf,

$$c = \int_{\hat{m}_{\min}}^{\hat{m}_{\max}} \mathrm{d}\hat{m}\, \exp\bigl[N I_N(\hat{m},\beta)\bigr]. \tag{31}$$

   Then the effective potential is

$$\Omega_N(\hat{m},\beta) = I_N(\hat{m},\beta) - \frac{1}{N}\log c. \tag{32}$$

6. Compute the canonical averages with the interpolated tethered averages and equation (28). The statistical errors are easily estimated with the jackknife method (see, e.g., [1]). The $i$th block of our splines interpolates the $i$th jackknife blocks of each simulated tethered mean value.
7. To obtain canonical results with a magnetic field $h$, simply substitute $\Omega_N$ with $\Omega_N^h$,

$$\Omega_N^h(\hat{m},\beta,h) = \Omega_N(\hat{m},\beta) + h\hat{m} - \frac{1}{N}\log c', \tag{33}$$

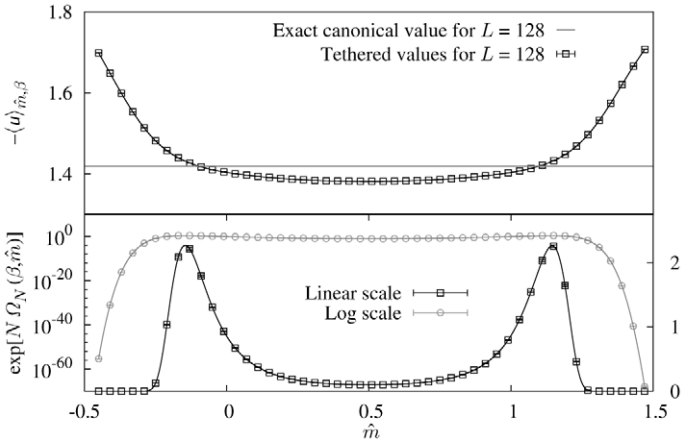


Fig. 1. Computation of the canonical average from tethered averages at the critical temperature. The lower panel depicts the pdf of $\hat{m}$, in logarithmic (left axis) and linear (right axis) scales, so that both the peaks and the tails can be seen. On the upper panel we plot the tethered mean values $-\langle u\rangle_{\hat{m},\beta_c}$ as a function of $\hat{m}$. The horizontal line is the exact value for $L = 128$ computed from [26], $\langle u\rangle_{\beta_c} = -1.419076\ldots$ The continuous curves are our cubic spline interpolations (see Appendix A). Our final result is $\langle u\rangle_{\beta_c} = -1.41905(5)$. Notice that the range of tethered values for $\langle u\rangle_{\hat{m},\beta_c}$ is several orders of magnitude greater than our statistical error.

where $c'$ is the new normalisation constant and use

$$\langle O\rangle_\beta(h) = \int \mathrm{d}\hat{m}\, \mathrm{e}^{N\Omega_N^h(\hat{m},\beta,h)}\langle O\rangle_{\hat{m},\beta}. \tag{34}$$

Fig. 1 pictures this process. On the top panel we represent the energy density as a function of $\hat{m}$, together with a horizontal line marking the canonical average at the critical point. On the bottom panel we plot the pdf $p(\hat{m})$. This function is reconstructed with great precision (we have to keep in mind that there is a factor $N = L^2$ in the exponent). The rendered accuracy in $p(\hat{m})$ allows us to obtain $\langle u\rangle_{\beta_c} = -1.41905(5)$, correct to five significant figures, even though the range of variation of $\langle u\rangle_{\hat{m}}$ is of $\sim 20\%$. The graphs were generated from the simulations described in Section 5.1.

Once the values of $\hat{m}$ have been selected, the independent simulations are carried out in a standard way. We use Metropolis dynamics to update the configuration. Let $\{\sigma_{\boldsymbol{x}}\}$ be the initial configuration and $\{\sigma'_{\boldsymbol{x}}\}$ the proposed new configuration (where one of the spins has been reversed). Then the probability of accepting the change is, from (23),

$$P\big(\{\sigma_{\boldsymbol{x}}\}\to\{\sigma'_{\boldsymbol{x}}\}\big) = \begin{cases} 0, & \text{if } M' > \hat{M}, \\ \min\{1, \mathrm{e}^{\Delta S}\}, & \text{if } M' \leqslant \hat{M}, \end{cases} \tag{35}$$

where

$$\Delta S = -\beta(U' - U) + \left(\frac{N}{2} - 1\right)\log\left(1 - \frac{M' - M}{\hat{M} - M}\right). \tag{36}$$

An interesting point about our algorithm is that it is 'compulsory parallel'. The fact that we have to run simulations at several values of $\hat{m}$ adds a layer of trivial parallelisation: we simply perform the simulations for each $\hat{m}$ independently and only later combine their results to construct $\Omega_N$ (an operation that is essentially costless in computer time).

A cautionary note: as our pseudorandom number generator we were originally using a 64 bit congruential generator reported in [32]. We simulated the lattice sequentially and extracted a random number per site, although in principle we would only need one when $\Delta S < 0$ in (36). This matches the conditions studied in [32,33], where significant deviations from the expected values were found using the same generator for a $D = 3$ Ising model. The error showed up only for large lattices, $N \geqslant 128^3$. Perhaps unsurprisingly, we also obtained wrong results (farther than 3 standard deviations from the exact values) for a system with a similar number of spins ($N = 1024^2$). This is our biggest system and we did not have any problems for all the smaller ones. Once this issue was identified, we added to the congruential generator a 64 bit version of the shift register method reported in [34] and redid all our computations. All the numerical results presented in this paper have been obtained using the sum of both generators (modulo $2^{64}$).

### 3.1. How to select a good sampling of $\hat{m}$

A good choice of the $\hat{m}$ we are going to simulate may reduce systematic and statistical errors significantly. Remember that while $-1 \leqslant m \leqslant 1$, $\hat{m}$ in principle may extend to infinity. Actually, $p(\hat{m})$ has completely negligible values outside the range $[-1/2, 3/2]$, so we can restrict ourselves to that interval. If we look at Fig. 1 we see that $p(\hat{m})$ is a two peaked distribution, so values of $\hat{m}$ inside the peaks contribute more that those in the middle or in the tails. These peaks get closer together and slightly narrower as we increase $L$, so it may seem that the choice of $\hat{m}$ is quite delicate (specially considering we do not know $p(\hat{m})$ until we have run our simulation).[4] A different, but related, question also arises: is it better to compute $\langle \hat{h} \rangle_{\hat{m},\beta}$ at more points or more precisely with a coarser grid? We shall try to give some practical recipes below.

The question is easy to analise for $I_N$, see Eq. (30). Let us assume that we have obtained the mean value of $\hat{h}$ at $K$ points in a grid. Our estimator $[\hat{h}]_k$ is related to the actual value by

$$[\hat{h}]_k = \langle \hat{h} \rangle_k + \eta_k, \quad k = 1, \ldots, K, \tag{37}$$

where $\eta_k$ are the errors, expected to be Gaussian distributed, of similar size and statistically uncorrelated. Hence, our numerical estimate for $I_N$ will be given by a quadrature formula

$$I_N \simeq \sum_{k=1}^{K} g_k \langle \hat{h} \rangle_k + \sum_{k=1}^{K} g_k \eta_k. \tag{38}$$

In this equation the first summand is subject to systematic error while the second one is the statistical error. Now, since the quadrature coefficients $g_k$ scale as $1/K$, it is clear that the statistical error will scale as $1/\sqrt{K}$. This suggests that doubling the number of points of the grid is equivalent to doubling the simulation time for each one. However, the analysis for canonical mean values is fairly more involved, since the errors in $\Omega_N$ will be highly correlated for different $\hat{m}$. Therefore, we perform a numerical experiment.

Table 1 shows the values for the energy density at the critical point, $-\langle u \rangle_{\beta_c}$, obtained in different series of runs. In the first column, we use evenly spaced points with $10^6$ Monte Carlo Sweeps (MCS) each. In the second column the points are also uniformly distributed, but now we perform $10^7$ MCS in each of them. The third and fourth columns are analogous, but with a greater density of points inside the peaks. We can reach several conclusions from this table:

[4] The discussion in this section is relevant to the disordered phase and the critical region. In the broken symmetry phase, the peaks rapidly get very high and extremely narrow as we increase $L$ and the criteria are different (see Section 8).

Table 1
Final value for $-\langle u\rangle_{\beta_c}$ as we change the number of points for the reconstruction of $\Omega_N$ and their precision. MCS = Monte Carlo Sweeps for each point. The runs labelled 'uniform sampling' consist of $N_{\text{points}}$ values of $\hat{m}$ evenly distributed in the range $[-0.4, 1.4]$. The runs labelled 'improved sampling' have $2/3N_{\text{points}}$ points evenly distributed in the same range, plus and additional $N_{\text{points}}/3$ inside the peaks, effectively doubling the density in the dominant regions. The last results of each column have a similar precision, but those computed with uniform sampling required twice the simulation time

| $N_{\text{points}}$ | Uniform sampling | | Improved sampling | |
|---|---|---|---|---|
| | $10^6$ MCS | $10^7$ MCS | $10^6$ MCS | $10^7$ MCS |
| 12 | 1.43728(33) | 1.43738(11) | | |
| 23 | 1.41925(22) | 1.419117(6) | | |
| 46 | 1.41921(13) | 1.419117(43) | 1.41908(11) | 1.419107(38) |
| 91 | 1.41914(10) | 1.419093(36) | 1.41913(8) | **1.419128(31)** |
| 181 | 1.41914(7) | **1.419095(28)** | 1.419034(5) | |
| 451 | 1.41906(5) | | 1.419073(39) | |
| 901 | 1.419065(33) | | **1.419077(26)** | |
| 1801 | **1.419062(24)** | | | |
| Exact | | 1.419076272086... | | |

- If we use too low a number of points we will see a significant systematic error, no matter how precise they are.
- Once the systematic error is under control, increasing the number of evenly distributed points has an effect of $1/\sqrt{N_{\text{points}}}$ in the statistical error. This is best seen in the leftmost column. The effect is roughly the same if we increase the number of MCS in each point by the same factor (the errors of the first column are $\sim\sqrt{10}$ times greater than the corresponding ones of the second).
- If we add more points inside the peaks, the error may decrease faster than $1/\sqrt{N_{\text{points}}}$. The errors with $N_{\text{points}}$ and uniform sampling are only slightly smaller than those with $N_{\text{points}}/2$ and improved sampling.

We can summarise this analysis with the following prescription for the choice of $\hat{m}$:

1. Run a first simulation with enough uniformly sampled $\hat{m}$ so that the systematic error is small or unnoticeable (i.e., so that the peaks of the distribution can be roughly reconstructed and the tails are reliably sampled). We have used $\sim 50$. This may seem a big number, but we must take into account that we have only looked at the energy in Table 1. Other quantities, such as high moments of the magnetisation or observables at a nonzero magnetic field, require that the tails of the distribution be reasonably well sampled.
2. Add a similar number of points inside the peaks of the pdf to eliminate the systematic error and reduce the statistical error.

We have found that the second step is not always necessary. In fact, for lattices up to $L = 256$ we have limited ourselves to computing 51 evenly distributed $\hat{m}$. For bigger lattices the peaks are steeper and we have added another 26 points inside them.

### *3.2. Other practical recipes*

It is sometimes interesting to compute high moments of the magnetisation (for example, see Section 6). One obvious possibility is to simply measure individual values for $m^\ell(\hat{m}; \{\sigma_x\})$ and

then compute the tethered and canonical averages as usual. But our method provides an alternative way of calculating $\langle m^\ell \rangle_\beta$. Indeed, we have the whole pdf $p(\hat{m})$ and we know that $\hat{M} = M + R$. Now, the moments for $R$ can be easily obtained analytically, so it suffices to compute $\langle \hat{m}^\ell \rangle_\beta$ to reconstruct $\langle m^\ell \rangle_\beta$ without any need for individual measurements of $m^\ell$. For example,

$$\langle m^2 \rangle_\beta = \langle (\hat{m} - 1/2)^2 \rangle_\beta - \frac{1}{2N}, \tag{39}$$

$$\langle m^4 \rangle_\beta = \langle (\hat{m} - 1/2)^4 \rangle_\beta - \frac{3}{N} \langle m^2 \rangle_\beta - \frac{3}{4N^2} + \frac{3}{N^3}. \tag{40}$$

These formulas are valid for the symmetric phase, where $\langle m \rangle_\beta = 0$. We have computed the moments of the magnetisation up to $\langle m^8 \rangle_\beta$ both from individual measurements and with this procedure and the results are identical. This will not be at all surprising once we see Section 4, where it is shown that the correlation time for $\langle m \rangle_{\hat{m},\beta}$ is $< 1$ (which means that the uncertainty in $p(\hat{m})$ is going to determine the total error).

## 4. Critical slowing down

Before we examine our results, we must make sure that we have been able to thermalise our systems and that we have enough independent measurements to generate precise averages. We would also like to know whether our algorithm suffers from critical slowing down (CSD) and, if so, in what measure.

To address these questions we have computed the autocorrelation functions and integrated autocorrelation times [1,5] for $u$, $\hat{h}$, $m$ and for each value of $\hat{m}$ (we will restrict ourselves to the critical temperature in this section). Another observable will be of interest. Remembering definitions (9) and (12), we can introduce the tethered mean value of the two point propagator at the smallest momentum:

$$\langle F \rangle_{\hat{m},\beta} = \frac{1}{N} \sum_{\boldsymbol{n}} \langle \sigma_{\boldsymbol{x}} \sigma_{\boldsymbol{0}} \rangle_{\hat{m},\beta} \mathrm{e}^{\mathrm{i}\boldsymbol{k}_1 \cdot \boldsymbol{x}}. \tag{41}$$

We define the autocorrelation function at time $t$ for an observable $O$ by

$$C_O(t, \hat{m}) = \langle O_s O_{s+t} \rangle_{\hat{m}} - \langle O \rangle^2_{\hat{m}}, \qquad \rho_O(t, \hat{m}) = \frac{C_O(t, \hat{m})}{C_O(0, \hat{m})}. \tag{42}$$

From this function we can obtain several characteristic times [5]:

$$\tau_{\mathrm{exp},O}(\hat{m}) = \lim_{t \to \infty} \sup \frac{t}{-\log |\rho_O(t, \hat{m})|}, \quad \text{exponential time of } O, \tag{43}$$

$$\tau_{\mathrm{exp}} = \sup_O \tau_{\mathrm{exp},O}, \quad \text{exponential time of the system}, \tag{44}$$

$$\tau_{\mathrm{int},O}(\hat{m}) = \frac{1}{2} + \sum_{t=1}^{\infty} \rho_O(t, \hat{m}), \quad \text{integrated time of } O. \tag{45}$$

The first two measure the amount of time (i.e. number of Monte Carlo sweeps) that must pass before the system is thermalised. The third characterises the minimum time difference so that two measurements can be considered independent (i.e. uncorrelated).

We compute $\tau_{\mathrm{int},O}$ using the self consistent window method [5]. In Fig. 2 we show the integrated autocorrelation times for $F$ and $\hat{h}$ as a function of $\hat{m}$.

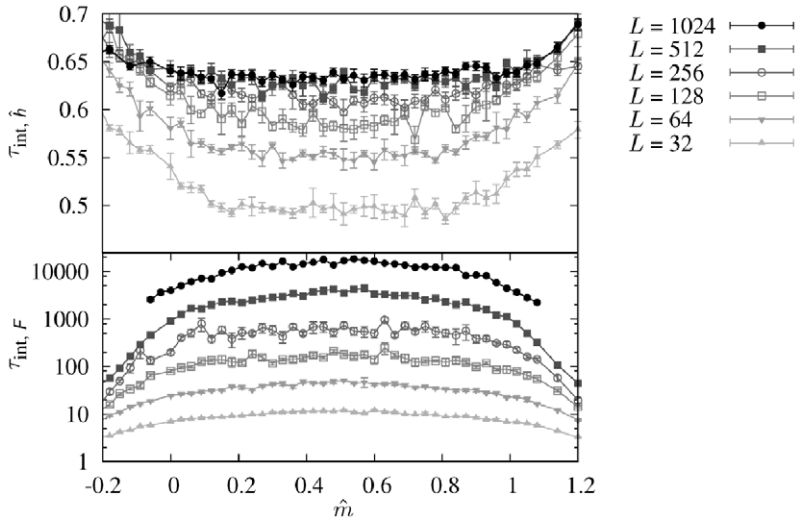


Fig. 2. Integrated autocorrelation time for $\hat{h}$ and $F$ as a function of $\hat{m}$, computed with the self consistent window method [5]. Notice the absence of critical slowing down for the former. In the lower panel, as the correlation time for $F$ grows as $L^2$, we did not use individual measurements of $F$ after each Monte Carlo step for $L \geqslant 512$. Instead, we averaged over 50 such measurements for $L = 512$ and over 4000 measurements for $L = 1024$. We then computed the autocorrelation functions for these blocked measurements (of course, we multiplied the integrated times thus obtained by the length of the blocks). This accounts for the smaller errors in $\tau_{\mathrm{int}}$ for these lattices. For $L = 1024$ the correlation time becomes unmeasurable (i.e., smaller than our blocks) for $\hat{m} > 1.1$ or $\hat{m} < -0.1$.

We see a clear difference: while the time scales for $F$ grow as $L^z$, with $z \approx 2$; the $\tau_{\mathrm{int}}$ for $\hat{h}$ do not exhibit any significant increase. That is, even though we are using a local algorithm, some of our observables do not experience any critical slowing down (and $\hat{h}$ is a particularly important observable, as we integrate it to obtain the effective potential). The integrated times for the energy are much smaller than those of $F$, but their behaviour is qualitatively similar (i.e., they grow as $L^2$). Within the computed quantities, $F$ is the slowest mode for our algorithm. In some sense, the absence of CSD for all functions of $m$ (including $\hat{h}$) is not completely surprising, because the Metropolis update uses nonlocal information that involves the whole system through $m$.

The exponential times are much more difficult to compute precisely, but we can easily give a rough estimate. Fig. 3 shows the normalised autocorrelation functions for the energy and $F$ at two different values of $\hat{m}$ (one at one of the maxima of $p(\hat{m})$, the other at the minimum). We see that $F$ is a rather pure mode for our Metropolis dynamics, with a very clean exponential decay for small times, so that $\tau_{\mathrm{exp},F} \approx \tau_{\mathrm{int},F}$. The curve for the energy falls rapidly at first and then becomes parallel to $\rho_F(t, \hat{m})$. This is a clear indication that the integrated time for $F$ can be considered as a good approximation to the exponential (i.e. thermalisation) time of the system.

The reader may find this section in conflict with the exact result by Hohenberg and Halperin [35], who showed that for conserved order parameter dynamics (model $B$) in Ising models the critical exponent is $z = 4 - \eta$. Nevertheless, even our slowest mode has a much smaller $z$. The way out of this paradox is in the nonlocal nature of our conservation law. Model $B$ needs magnetisation diffusion across the boundary if the magnetisation is to change in the enclosed region. When the locality constraint is violated, the new dynamical exponent is expected to be $z_{\mathrm{nonlocal}} = z - 2$ [36]. Clearly, this is the case for our dynamics, where a change of $\hat{m}$ inside a given region does not occur through diffusion across its boundary.

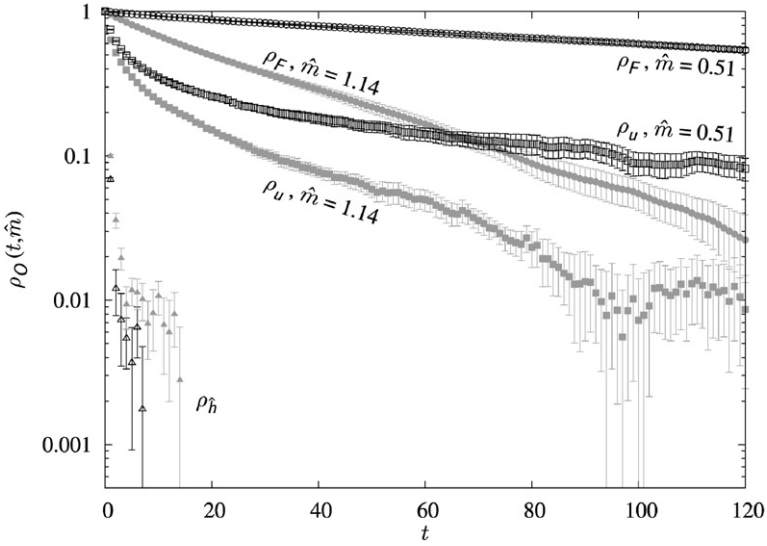


Fig. 3. Normalised autocorrelation functions of $u$, $F$ and $\hat{h}$ at the minimum ($\hat{m} = 0.51$, black symbols) and one of the maxima ($\hat{m} = 1.14$, grey symbols) of $p(\hat{m})$ for $L = 128$ at the critical temperature. We appreciate how the curves for $u$ (circles) and $F$ (squares) become parallel after a small number of steps. We have only plotted $\rho_{\hat{h}}$ (triangles) until the point where it first becomes compatible with zero, to avoid cluttering the graph.

## 5. Results at $\beta_c$, $h = 0$

We summarise here our results at the critical point, which correspond to the bulk of our simulations. This section is divided in three parts. First we provide the parameters of our simulations. Second, we report our results for the mean values that would be considered in a traditional canonical computation. Finally, in Section 5.3 we perform a rather unconventional, but very accurate, computation of the critical exponents ratio $\beta/\nu$ taking advantage of the peculiarities of the tethered formalism.

### *5.1. Parameters of our simulations*

We have simulated lattice sizes $L = 16, 32, \ldots, 1024$. For systems with $L \leqslant 256$ we have used 51 uniformly distributed values of $\hat{m}$ in $[-0.5, 1.5]$ (except for $L = 16$, where we had to extend the range to $[-1.61, 1.61]$ to avoid cutoff errors). As we shall see in Table 2, this choice (considered suboptimal in Section 3) does not introduce any discernible systematic error. We have been very conservative and chosen a wider range for $\hat{m}$ than what we used in Section 3.1, slightly enlarging the computations to avoid any chance of a cutoff error. For $L \geqslant 512$ we ran a first simulation with 51 equally spaced $\hat{m}$ in $[-0.3, 1.3]$. In these cases the peaks were considerable narrower and closer together than for the smaller lattices. To avoid any discretisation errors, we have followed the practical recipe given in Section 3: after obtaining an approximation to the shape of $\Omega_N$, we have added another 26 points, doubling the density inside the peaks.

In all cases we have performed $10^7$ Metropolis sweeps for each value of $\hat{m}$. Following the standard prescription [5], we have discarded a fifth of the measurements for thermalisation (although the correlation times are much smaller, see Section 4) and formed 100 jackknife blocks [1] with the rest to obtain a reliable estimate of the statistical error. According to Section 4 and, partic-

Table 2
Results at the critical temperature and comparison with a cluster algorithm. (T): Tethered Monte Carlo, (C): Swendsen–Wang, (E): Exact results at finite $L$ from [26]

| $L$ | $-\langle u\rangle_{\beta_c}$ | $\chi_2/L^2$ | $\xi_1/L$ | $\xi_2/L$ | $C$ | $B$ | $\partial_\beta \xi_1/10^4$ |
|---|---|---|---|---|---|---|---|
| 16 (T) | 1.45308(4) | 0.54543(6) | 0.9116(2) | 0.24613(13) | 7.7186(14) | 1.16562(7) | 0.036547(9) |
| 16 (C) | 1.4529(2) | 0.5451(3) | 0.9104(9) | | 7.718(10) | 1.165 9(3) | 0.03650(6) |
| 16 (E) | 1.453065... | | | | 7.717134... | | |
| 32 (T) | 1.43369(4) | 0.45900(10) | 0.9072(4) | 0.2422(3) | 9.509(3) | 1.16723(14) | 0.14407(7) |
| 32 (C) | 1.43367(12) | 0.4591(2) | 0.9078(9) | | 9.493(13) | 1.1671(3) | 0.1441(3) |
| 32 (E) | 1.433659... | | | | 9.509379... | | |
| 64 (T) | 1.42397(4) | 0.38619(18) | 0.9065(9) | 0.2400(5) | 11.285(6) | 1.1675(3) | 0.5738(6) |
| 64 (C) | 1.42390(6) | 0.3860(2) | 0.9056(10) | | 11.293(17) | 1.1677(4) | 0.5731(11) |
| 64 (E) | 1.423938... | | | | 11.288138... | | |
| 128 (T) | 1.41905(5) | 0.3244(3) | 0.9040(18) | 0.2408(11) | 13.063(10) | 1.1684(7) | 2.289(5) |
| 128 (C) | 1.41906(4) | 0.32459(17) | 0.9048(10) | | 13.06(2) | 1.1677(4) | 2.287(4) |
| 128 (E) | 1.419076... | | | | 13.060079... | | |
| 256 (T) | 1.41663(5) | 0.2728(6) | 0.904(4) | 0.240(2) | 14.83(2) | 1.1687(14) | 9.16(4) |
| 256 (C) | 1.41664(2) | 0.27286(14) | 0.9042(9) | | 14.83(2) | 1.1682(4) | 9.14(2) |
| 256 (E) | 1.416645... | | | | 14.828595... | | |
| 512 (T) | 1.41542(4) | 0.2293(7) | 0.903(6) | 0.240(4) | 16.57(3) | 1.168(2) | 36.38(19) |
| 512 (C) | 1.415444(11) | 0.22968(13) | 0.9059(10) | | 16.60(2) | 1.1676(4) | 36.64(10) |
| 512 (E) | 1.415429... | | | | 16.595404... | | |
| 1024 (T) | 1.41489(4) | 0.1949(15) | 0.919(15) | 0.240(10) | 18.28(8) | 1.163(6) | 148.8(19) |
| 1024 (C) | 1.414826(6) | 0.19307(12) | 0.9046(11) | | 18.35(3) | 1.1681(4) | 146.1(4) |
| 1024 (E) | 1.414821... | | | | 18.361348... | | |

ularly, Fig. 2, this means that for $L = 1024$ the length of the blocks is only about 5 times the largest found $\tau_{\text{exp}}$ (that of $\hat{m} = 0.5$). There has been no need to increment the numerical effort in this point as this exponential time corresponds to the minimum of $p(\hat{m})$ and we have seen that the canonical values are dominated by the neighbourhood of the peaks. There the exponential time is an order of magnitude smaller, so our error estimates are sound (as can be seen by comparing our results with the exact values). In any case, we have recomputed the errors of Table 2 with 50 and 200 jackknife blocks and checked that they remain completely stable. Our canonical simulations consisted of $10^7$ Swendsen–Wang updates.

### 5.2. *Canonical averages at the critical temperature and zero field*

We present in Table 2 our values for the canonical averages of several physical quantities. We have compared with the exact results for $u_\beta$ and $C$ in finite lattices computed with the expressions given by Ferdinand and Fisher [26]. We have also run simulations with a Swendsen–Wang cluster algorithm (we use our own implementation, based on the one distributed with [1], but our results are compatible with those of [37]).

From Table 2 we can confirm that TMC is capable of producing very accurate results. The relative errors for $\chi_2$ and $B$ scale as $L$. This can be accounted for by noticing that both are completely determined by $p(\hat{m})$, recall Section 3.2. Indeed, while $\hat{h}$ is self averaging and virtually free of critical slowing down (meaning that for a fixed simulation length its error scales as $1/\sqrt{N}$), we are multiplying $\Omega_N(\hat{m}, \beta)$ by a factor of $N$, yielding an overall $\sqrt{N}$ scaling for the errors.

As we said in the Introduction, TMC is not meant to be a competitor to cluster algorithms for the Ising model without magnetic field. For example, the CPU time to compute each of the 77

simulations at fixed $\hat{m}$ for $L = 1024$ is about a third of what we needed for the whole Swendsen–Wang simulation, which is also more precise.

### 5.3. Finite size scaling and the peaks of $p_1(m)$

Let us obtain an accurate estimate of the critical exponent ratio $\beta/\nu$ (known to be $1/8$) in a way that would not be competitive for a canonical computation.

Our starting point is the Finite Size Scaling formula for an arbitrary observable $\mathcal{O}$ (see, e.g., [1]), as we get closer to the critical point ($\beta = \beta_c$, $h = 0$):

$$\langle \mathcal{O} \rangle_t(h) = L^{-x_{\mathcal{O}}/\nu} \left[ f_{\mathcal{O}}\left(L^{1/\nu} t, L^{y_h} h\right) + \cdots \right], \quad t = \frac{\beta_c - \beta}{\beta_c}. \tag{46}$$

Here the dots represent possible corrections to scaling. We shall work at $h = 0$, so we only have to consider the first argument of the scaling function $f_{\mathcal{O}}$.

Elaborating equation (46) and recalling that $\beta$ is the critical exponent for the magnetisation, it can be shown that (see, e.g., [1])

$$\tilde{p}_1(m, \beta_c; L) = L^{\beta/\nu} \tilde{f}\left(L^{\beta/\nu} m\right), \tag{47}$$

where $\tilde{p}_1(m, \beta_c; L)$ is some smoothed version of $p_1(m, \beta_c; L)$, Eq. (16). Recalling that $p(\hat{m}, \beta_c; L)$, Eq. (20), is just one of such smoothings, we can substitute this expression by

$$p(\hat{m}, \beta_c; L) = L^{\beta/\nu} f\left(L^{\beta/\nu} (\hat{m} - 1/2)\right). \tag{48}$$

In particular, the pdf has two maxima at $m^{\pm}_{\text{peak}} + \frac{1}{2}$, whose scaling behaviour is expected to be $m^{\pm}_{\text{peak}} \propto L^{-\beta/\nu}$.

Recall that we measure directly $\hat{h}$, which is the derivative of the logarithm of $p(\hat{m})$ and thus is exactly zero at these peaks. Therefore, for each of the maxima we just have to identify the two consecutive points of the grid such that $\langle \hat{h} \rangle_{\hat{m}_i, \beta} > 0$ and $\langle \hat{h} \rangle_{\hat{m}_{i+1}, \beta} < 0$ and find the root of the cubic spline joining them (we have also used jackknife blocks to estimate the errors).

The position of these peaks is a canonical observable, but one that is more easily obtained through the tethered ensemble (in a canonical simulation we would have had to construct $p_1(m)$ and locate its maximum directly, a harder problem than finding a zero).

The results of this analysis for the simulations described in Section 5.1 are collected in Table 3. Notice that even with our relatively coarse $\hat{m}$ sampling we have been able to determine the position of the peaks with a precision ranging from 0.013% to 0.46%. If we had wanted to give a very precise value for these points, we could have done so with a rather small investment in CPU time, as we only need precise simulations at two values of $\hat{m}$, conveniently chosen.

By fitting $m^{\pm}_{\text{peak}}(L)$ to a power law we can obtain an estimate of $\beta/\nu$. Table 4 gathers the results of fitting the data of Table 3 to a power law, for lattice sizes $L \geqslant L_{\text{min}}$. We see that for $L_{\text{min}} = 32$ the power law does not represent the curve adequately. To give an error estimate that represents both systematical and statistical sources we follow the criterion explained in [38]: when two consecutive values are first compatible, we give the most precise as central value, but with the bigger error. For the negative magnetisation peak we find $\beta/\nu = 0.1239(11)$ and for the positive peak $\beta/\nu = 0.1245(10)$.

Following [37], we can even go further and try to characterise the corrections to scaling. We assume that in the Ising model in $D = 2$ the dominant corrections to scaling are analytical

$$m^{\pm}_{\text{peak}} = L^{-\beta/\nu} \left[ A^{\pm} + B^{\pm} L^{-\Delta} \right], \quad \Delta = 7/4. \tag{49}$$

Table 3
Position of the peaks of the probability density function of the magnetisation for several lattice sizes. As we are at the critical point, the values in the table extrapolate to zero when $L \to \infty$ (compare with Section 8, where we study the ferromagnetic region)

| $L$ | $-m^{-}_{\text{peak}}$ | $m^{+}_{\text{peak}}$ |
|---|---|---|
| 32 | 0.76401(10) | 0.76431(11) |
| 64 | 0.70286(18) | 0.7030(2) |
| 128 | 0.6453(3) | 0.6451(4) |
| 256 | 0.5921(7) | 0.5910(7) |
| 512 | 0.5419(12) | 0.5427(9) |
| 1024 | 0.499(2) | 0.500(2) |

Table 4
Fits of $m^{\pm}_{\text{peak}}(L)$ to a power law, $m^{\pm}_{\text{peak}} = AL^{-x}$, including all lattice sizes $L \geqslant L_{\min}$. We give the computed exponent and the chi square per degree of freedom. As discussed in the text, for small lattices we detect corrections to scaling. Our fits converge to the exact result, $\beta/\nu = 0.125$

| $L_{\min}$ | $m^{-}_{\text{peak}}$ | | $m^{+}_{\text{peak}}$ | |
|---|---|---|---|---|
| | $\beta/\nu$ | $\chi^2$/d.o.f. | $\beta/\nu$ | $\chi^2$/d.o.f. |
| 32 | 0.1217(3) | 23.44/4 | 0.1224(3) | 27.85/4 |
| 64 | 0.1239(5) | 2.027/3 | 0.1245(5) | 2.087/3 |
| 128 | 0.1250(11) | 0.7569/2 | 0.1246(10) | 2.053/2 |
| 256 | 0.126(4) | 0.6456/1 | 0.1220(23) | 0.3248/1 |

We have fitted our points for all lattices to this expression, fixing the exponents to their exact values and varying $A^{\pm}$ and $B^{\pm}$. We have obtained $\chi^2/\text{d.o.f.} = 0.9858/4$ for the negative peak and $\chi^2/\text{d.o.f.} = 2.825/4$ for the positive one.

## 6. The scaling paramagnetic region: The renormalised coupling constants

We shall show here that TMC works as well in the paramagnetic phase in the scaling region. For definiteness, we shall study the renormalised coupling constants (see [2,3]). These constants are notoriously difficult to compute using Monte Carlo methods, so they provide a good challenge for our formalism.

Let us consider the $D = 2$ Ising model in its thermodynamical limit. Then we can define the Gibbs free energy by

$$G(t,h) = \lim_{N\to\infty} \frac{1}{N} \log\bigl[Z(t,h)\bigr], \quad t = \frac{\beta_c - \beta}{\beta_c} \tag{50}$$

and its Legendre transform, the Helmholtz free energy ($m_t = \langle m \rangle_t$),

$$F(t,m_t) = \max_h \bigl[m_t h - G(t,h)\bigr]. \tag{51}$$

From a field theoretical point of view, the latter can be expanded as a series in the renormalised coupling constants $g_{2n}$ (here we shall use the definitions of [39])

$$F(t,m_t)-F(t,0)=\frac{1}{\xi^2}\left(\frac{1}{2}\phi^2+\sum_{n=2}^{\infty}\frac{g_{2n}}{(2n)!}\phi^{2n}\right) \tag{52}$$

$$=-\frac{\chi_2^2}{\chi_4}\left(\frac{1}{2}z^2+\frac{1}{4!}z^4+\sum_{n=3}^{\infty}\frac{r_{2n}}{(2n)!}z^{2n}\right). \tag{53}$$

In these equations,

$$\phi^2=\frac{\xi(t)^2}{\chi_2(t)}m_t^2,\qquad z^2=-\frac{\chi_4(t)}{\chi_2(t)^3}m_t^2. \tag{54}$$

We would like to express the $g_{2n}$ in a form suitable for our lattice simulations. To do this we remember definition (15), according to which $G(t,h)$ can be immediately represented as a Taylor expansion with coefficients $\chi_{2n}$,

$$G(t,h)-G(t,0)=\sum_{n=1}^{\infty}\frac{\chi_{2n}}{(2n)!}h^{2n}. \tag{55}$$

Combining all these equations we arrive at the following explicit formulas:

$$g_4=-\lim_{t\to 0^+}\frac{\chi_4(t)}{\chi_2(t)^2\xi(t)^2},\qquad g_{2n}=r_{2n}(g_4)^{n-1}, \tag{56}$$

with

$$r_6=10-\lim_{t\to 0^+}\frac{\chi_6(t)\chi_2(t)}{\chi_4(t)^2}, \tag{57}$$

$$r_8=280+\lim_{t\to 0^+}\left[\frac{\chi_8(t)\chi_2(t)^2}{\chi_4(t)^3}-56\frac{\chi_6(t)\chi_2(t)}{\chi_4(t)^2}\right]. \tag{58}$$

There has been a great deal of interest about these coupling constants and many precise computations have been performed, both with field theoretical and numerical methods. Balog et al. [40] arrive at $g_4=14.6975(1)$ with a form factor approach while Caselle et al. [39] give $g_4=14.697323(20)$, $r_6=3.67866(3)(2)$ and $r_8=26.041(8)(3)$ using transfer matrix techniques. There are fewer Monte Carlo determinations of these quantities [40,41].

In this section we shall reproduce the Monte Carlo computations of [41] with the TMC method to give our own estimate of the first coupling constants. A Monte Carlo determination of the $g_{2n}$ can obviously not be directly computed for an infinite lattice. Instead, we have to perform a double limit $\lim_{t\to 0^+}\lim_{L\to\infty}$, that is, run simulations very close to, but above, the critical temperature at increasing values of $L$ until the results are stable (within our errors). Ref. [41] concludes that $L=100$ is a big enough lattice. In order to compare our results to those of that reference, we have worked at the same temperature, $\beta=0.42$.

We have used 191 uniformly spaced $\hat{m}$ in $[-0.45, 1.45]$, with $10^7$ Monte Carlo sweeps each. Table 5 summarises our results, which are compatible with those of [41] but more precise. These calculations involve working with high moments of the magnetisation (we have used the indirect method explained in Section 3.2, combining the cumulants of $r$ and $\hat{m}$). The table also compares the tethered results with a Swendsen–Wang simulation (SW). Notice that in the latter the errors increase very quickly when we consider high powers of $m$. For instance, for $L=100$ the error in the susceptibility is almost the same for the TMC and the SW methods, while for $g_8$ the error of the latter is almost ten times higher. Our whole TMC simulation for $L=100$ required about 100 hours of computer time, while the Swendsen–Wang one was completed in about 10. If we use

Table 5
The renormalised coupling constants. TMC: Tethered Monte Carlo; SW: Swendsen–Wang; SWC: Swendsen–Wang with cluster estimators. For $L = 100$ we also give the results of Ref. [41], computed with a single cluster Monte Carlo method

| | $L = 50$ | | | $L = 100$ | | | |
|---|---|---|---|---|---|---|---|
| | TMC | SW | SWC | TMC | SW | SWC | Ref. [41] |
| $-\langle u\rangle_\beta$ | 1.228238(14) | 1.22831(4) | | 1.226067(7) | 1.226076(8) | | |
| $\chi_2$ | 196.85(9) | 196.96(15) | 196.91(5) | 203.78(11) | 204.07(10) | 203.92(2) | 204.4(3) |
| $\xi_1$ | 11.749(5) | 11.756(9) | 11.753(3) | 11.888(11) | 11.907(10) | 11.8932(10) | 11.90(2) |
| $r_6$ | 4.4462(9) | 4.449(4) | 4.4469(10) | 3.70(6) | 3.73(8) | 3.731(6) | |
| $r_8$ | 39.76(3) | 39.83(13) | 39.77(3) | 26.2(6) | 24(3) | 26.47(18) | |
| $g_4$ | 12.817(6) | 12.80(3) | 12.812(7) | 14.66(5) | 14.69(9) | 14.673(8) | 14.60(16) |
| $g_6$ | 730.4(5) | 729(3) | 729.9(9) | 794(9) | 806(24) | 803.3(16) | $8.5(4) \times 10^2$ |
| $g_8/10^4$ | 8.370(8) | 8.36(6) | 8.363(16) | 8.25(13) | 7.5(11) | 8.34(7) | 8.8(10) |

'improved' or cluster estimators (SWC) [42], however, the advantage of the tethered algorithm disappears.

## 7. Results at $\beta_c$, $h \neq 0$

An interesting feature of TMC is that it allows us to obtain accurate data in the presence of a magnetic field. In order to do this, we reanalise the data from the simulations described in Section 5.1. Let us stress the fact that we do not have to run any new simulations at all, we simply use the tethered values computed at zero magnetic field and modify the effective potential as in Eqs. (33) and (34).

We will typically be interested not in computing the equivalent of Table 2 for a particular value of $h$, but in drawing a curve $\langle O\rangle_\beta(h)$. When doing this, we can improve our statistical errors somewhat if we take into account that the observables can be either odd or even in $h$. This means that we can (anti)symmetrise the curves:

$$\langle O\rangle_\beta^{\text{odd}}(h) = \frac{\langle O\rangle_\beta(h) - \langle O\rangle_\beta(-h)}{2}, \tag{59}$$

$$\langle O\rangle_\beta^{\text{even}}(h) = \frac{\langle O\rangle_\beta(h) + \langle O\rangle_\beta(-h)}{2}. \tag{60}$$

Now, if the data were completely uncorrelated, so that $\langle O\rangle_\beta(\pm h)$ were independent, this operation would imply a $1/\sqrt{2}$ reduction in the statistical error. Actually, this is not the case: the individual values for $\pm h$ are very strongly correlated and the symmetrisation reduces only very slightly the error for even quantities. For odd observables, however, the fact that we are computing a difference rather than a sum yields a very significant decrease in the statistical error (around a factor of 10, specially for small values of $h$). We shall use Eqs. (59) and (60), but we shall drop the explicit 'odd' or 'even' superscripts.

The first observable we shall consider is the correlation length $\xi_2(h)$, defined in Eq. (13). This is even in $h$, so we can use the symmetrised version of Eq. (60). In this case, unlike previous sections, no data for $\xi_2(h)$ are readily available in a finite lattice and doing our own cluster simulations would be harder (as we pointed out in the Introduction, the currently most popular methods in the $h \neq 0$ regime are transfer matrix techniques). Nevertheless, we can provide a very good check of consistency using the FSS equation (46). Indeed, given that our simulations have been carried out at the critical temperature, we can consider the critical behaviour as $h \to 0$.

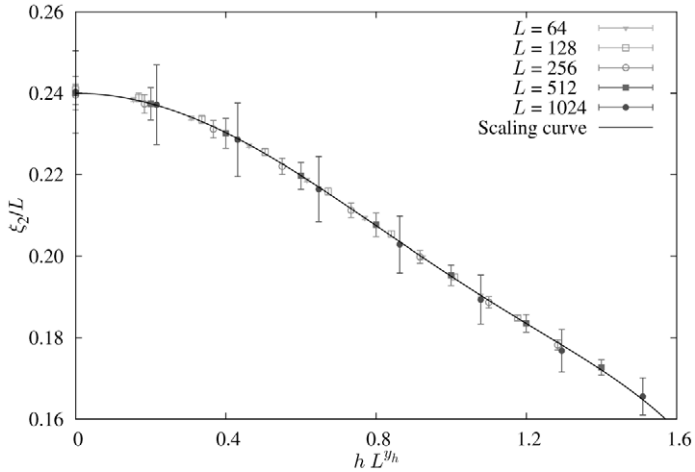


Fig. 4. Finite size scaling with $\xi_2(h)$. We represent the scaling function by a fit to $f_\xi(x) = a_0 + a_2x^2 + a_4x^4 + a_6x^6$. The value of the diagonal chi square per degree of freedom is $\chi^2_{\rm d}/\text{d.o.f} = 3.978/36$, which confirms that the points fall on a smooth curve within their errors.

In our case, we are working at precisely $\beta = \beta_{\rm c}$, so the first variable in the scaling function disappears and we have ($x_O = \nu$ for the correlation length)

$$\xi_2/L \simeq f_{\xi_2}\big(L^{y_h}h\big). \tag{61}$$

The critical exponent $y_h$ is 15/8 for the two-dimensional Ising model and the function $f_{\xi_2}$ is expected to be very smooth. As we can see in Fig. 4, Eq. (61) is perfectly valid in our case, once we discard the data for $L \leqslant 32$. At a first glance, it may seem that we have even overestimated our errors for $L = 1024$, but remember that the points are very strongly correlated. The universal scaling curve is well represented by a sixth order even polynomial, with a value of diagonal $\chi^2_{\rm d}$/d.o.f. of 3.978/36.[5]

Thus, the universal scaling function $f_{\xi_2}(x)$ for $x \lesssim 1.5$ is extremely well represented by[6]

$$f_{\xi_2}(x) = a_0 + a_2x^2 + a_4x^4 + a_6x^6, \tag{62}$$

with

$$a_0 = 0.2399(2), \qquad a_2 = -0.0639(4), \qquad a_4 = 0.0235(7), \qquad a_6 = -0.0045(4). \tag{63}$$

We now consider the magnetisation, $m_{\beta_{\rm c}}(h) = \langle m\rangle_{\beta_{\rm c}}(h)$. Contrary to the correlation length, the magnetisation is an odd function of $h$. This means that by antisymmetrising our results for $\pm h$ as in Eq. (59) we can greatly reduce the error. In this case we again lack a convenient way of generating the same curve with a different method, but we still can check the validity of our results. To do this, we differentiate equation (55) and notice that the coefficients of the Taylor

[5] The points of the graph are very strongly correlated, so their covariance matrix is singular and the $\chi^2$ parameter of the fit cannot be computed. Instead, we restrict ourselves to the diagonal elements of the covariance matrix and minimise the resulting 'diagonal' $\chi^2_{\rm d}$. Usually, the degrees of freedom are computed as number of points minus the number of parameters. In our case this does not correspond to the actual degrees of freedom of the fit, but we have maintained the usual notation.

[6] To estimate the errors we have computed a fit for each jackknife block.

Table 6
Nonlinear susceptibilities from direct measurements at $h = 0$ (M) and from a finite difference formula for $m_{\beta_c}(h)$ as a function of the magnetic field (F)

| $L$ | $N^{-1}\chi_2$ | $N^{-2}\chi_4$ | $N^{-3}\chi_6$ | $N^{-4}\chi_8$ |
|---|---|---|---|---|
| 16 (M) | 0.54543(6) | −0.54572(13) | 2.2657(8) | −20.059(10) |
| 16 (F) | 0.54543(6) | −0.5457(2) | 2.2628(19) | −19.70(14) |
| 32 (M) | 0.45900(10) | −0.3861(2) | 1.3485(10) | −10.042(10) |
| 32 (F) | 0.45900(10) | −0.3862(3) | 1.3484(18) | −10.00(2) |
| 64 (M) | 0.38619(18) | −0.2733(3) | 0.8031(13) | −5.032(11) |
| 64 (F) | 0.38619(18) | −0.2738(5) | 0.805(2) | −5.02(2) |
| 128 (M) | 0.3244(3) | −0.1928(4) | 0.4758(17) | −2.504(12) |
| 128 (F) | 0.3244(3) | −0.1943(7) | 0.481(3) | −2.52(2) |
| 256 (M) | 0.2728(6) | −0.1362(7) | 0.283(2) | −1.250(12) |
| 256 (F) | 0.2725(6) | −0.1358(15) | 0.280(6) | −1.20(4) |
| 512 (M) | 0.2293(7) | −0.0964(7) | 0.168(2) | −0.625(9) |
| 512 (F) | 0.2293(7) | −0.0960(12) | 0.166(4) | −0.60(2) |
| 1024 (M) | 0.1949(15) | −0.0698(13) | 0.104(3) | −0.328(12) |
| 1024 (F) | 0.194(3) | −0.063(6) | 0.08(2) | −0.2(3) |

expansion of $\langle m\rangle_{\beta_c}(h)$ are none other than the $2n$ point correlation functions at zero momentum:

$$m_{\beta_c}(h) = \langle m\rangle_{\beta_c}(h) = \frac{1}{N}\frac{\partial \log Z}{\partial h} = \chi_2 h + \frac{\chi_4}{3!}h^3 + \frac{\chi_6}{5!}h^5 + \frac{\chi_8}{7!}h^7 + \cdots. \tag{64}$$

This expansion provides a new way of computing $\chi_{2n}$: we just generate a reasonable number of points of the $m(h)$ curve, which we parameterise with a truncated version of Eq. (64). The choice of values for $h$ is somewhat delicate: if we use very small magnetic fields we will only be able to appreciate the first few coefficients but if we go too far in $h$ we would need to have sampled the tails of the pdf of $\hat{m}$ very precisely. We have found that magnetic fields up to $\sim (\chi_2)^{-1}$ provide a good compromise.

A second difficulty is that posed by the correlations among the points of the curve. These are so strong that the covariance matrix turns out singular, which bars us from obtaining a fit and its errors by minimising $\chi^2$. Instead, we have computed an odd interpolating polynomial with a finite difference formula (this gives us as many $\chi_{2n}$ as points) and we have tried to control the correlation by estimating the errors with the jackknife method. This takes care of the statistical error. To control the systematic error, we have both reduced the range in $h$ and varied the number of points to check whether the parameters were stable. We have found that if we use this method with $n$ points the last one or two coefficients are usually unreliable (i.e., their value changes beyond the error bars if we add another point). This only means that if we want to obtain $n$ physically meaningful parameters, we should compute at least $n + 2$ points. We want to compute the nonlinear susceptibilities up to $\chi_8$, so to be safe we have used 7 points for each lattice size, equally spaced at intervals of $(10\chi_2)^{-1}$, where $\chi_2$ is the susceptibility computed from the simulation at $h = 0$.

Table 6 summarises our results for the $\chi_{2n}$, computed from the measurements at $h = 0$ and from the finite difference formula at $h \neq 0$. We see that both series of values are compatible, but that the former are more precise.

We can also do a FSS analysis with the magnetisation. Notice that at small applied fields $m_\beta(h) \simeq \chi_2 h$. If we increase the field, however, we can appreciate a deviation from the linear behaviour (see the left graph of Fig. 5). If we want to collapse all the curves on one we must take

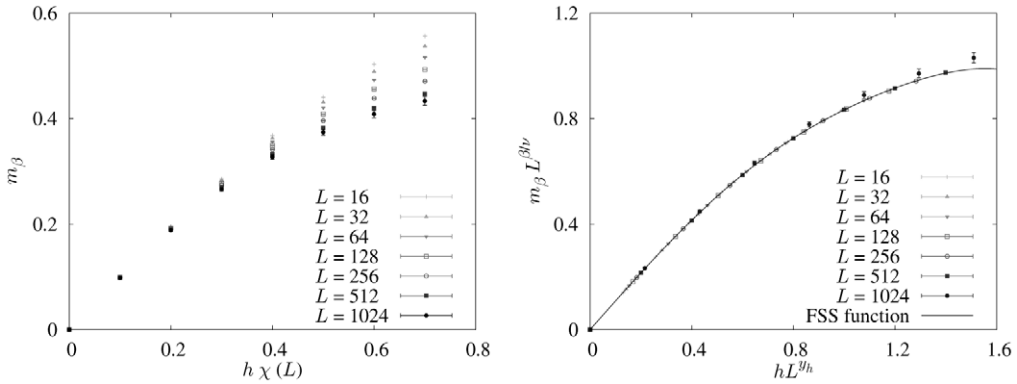


Fig. 5. Magnetisation at nonzero magnetic field for different lattice sizes. We provide two representations. The one on the left is plotted in terms of the applied field times the susceptibility at $h = 0$. This way we can appreciate the linear and nonlinear regimes. The graph on the right is the FSS curve for $m_\beta(h)$ (a fit to a seventh order odd polynomial, with diagonal $\chi^2_{\mathrm{d}}/\mathrm{d.o.f.} = 41.85/31$).

the critical exponent of the magnetisation, $-\beta$, into account:

$$m_{\beta_c}(h) \simeq L^{-\beta/\nu} f_m\big(L^{y_h} h\big). \tag{65}$$

The function $f_m$ is depicted on the right panel of Fig. 5. We fit it to an odd polynomial $f_m(x) = a_1 x + a_3 x^3 + a_5 x^5 + a_7 x^7$ for lattices $L \geqslant 64$, as we did for the correlation length. The value of the diagonal $\chi^2_{\mathrm{d}}/\mathrm{d.o.f.}$ for this fit is $41.85/31$. The last point of the curve, which corresponds to the highest magnetic field for $L = 1024$, seems to show a small deviation from the curve. The reason may be that we are taking the range of the scaling variable too far and that scaling corrections start to act. Remember that we had spaced the values of $h$ in units of $(10\chi_2)^{-1}$, so that the representation on the left scaled properly, which is not be best choice for the FSS analysis.

It is interesting to examine the behaviour of the magnetisation with small but $L$ independent magnetic fields (Fig. 6). We observe two well differentiated scales: an FSS regime, where the slope of the curve is very large, and a thermodynamic limit, where the curves merge. The range of $h$ is limited by the largest obtained $\langle \hat{h} \rangle_{\hat{m},\beta}$ in the simulated $\hat{m}$ grid (this is the reason for the rapid growth of the error bars for the final points, specially noticeable in the largest lattices). Due to the small value of $\beta/\nu$, the displacement of the curves for small $h$ is almost linear in $\log L$, see Eq. (65).

We can repeat the process described here for other observables, such as the energy or specific heat. However, our computation can be inefficient if we do not prepare it carefully. Remember that for $h = 0$ the canonical average was dominated by two peaks, whose position was determined by the value of $\hat{m}$ such that $\langle \hat{h} \rangle_{\hat{m}} = 0$. Now the value with a nonzero magnetic field will be even more dependent on a saddle point, determined by

$$\langle \hat{h} \rangle_{\hat{m}} = h. \tag{66}$$

In practice, this means that the way to obtain a precise result for, say, the energy at a given field $h$ is to first estimate the value of $\hat{m}$ such that the previous equation is satisfied and then run a long simulation there.

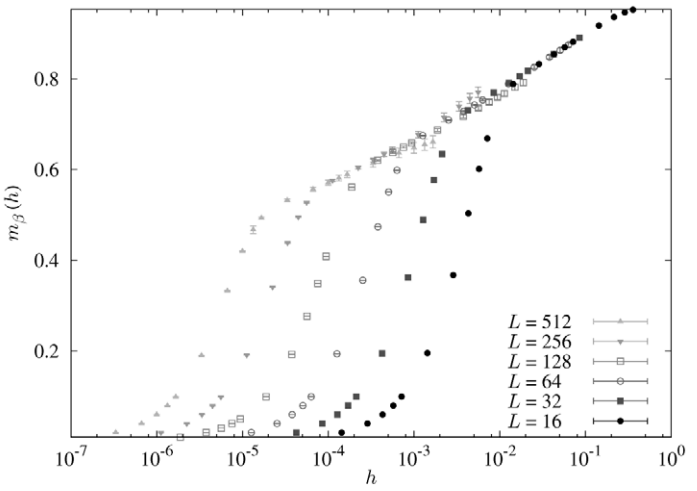


Fig. 6. Magnetisation at the critical point for several lattices and an $L$ independent range of magnetic field values (notice the logarithmic scale of the horizontal axis).

## 8. The broken symmetry phase

Let us now consider the $\beta > \beta_c$ regime. In this situation, the infinite system shows a nonzero expectation value for the order parameter, $m_{\beta>\beta_c} = \langle m \rangle_{\beta>\beta_c} \neq 0$, even in the absence of an external magnetic field. This may seem incompatible with the partition function (1), where the configurations $\{\sigma_{\boldsymbol{x}}\}$ and $\{-\sigma_{\boldsymbol{x}}\}$ occur with equal probability. The well known solution for this apparent paradox is spontaneous symmetry breaking [2], whose mathematical formulation involves considering a small magnetic field (which establishes a preferred direction) and taking the double limit

$$\langle m \rangle_{\beta,\infty} = \lim_{h\to 0} \lim_{L\to\infty} \langle m \rangle_{\beta,L}. \tag{67}$$

The order of the two limits is crucial: were we to reverse it the magnetisation would always vanish. We see then that the symmetry of our model complicates the definition of a broken symmetry phase for finite lattices in the canonical ensemble. The traditional workaround consists in considering not the magnetisation $m$, but its absolute value $|m|$.

The tethered ensemble provides a cleaner concept of broken symmetry phase. Consider the pdf of $\hat{m}$, as in Fig. 1. In the ferromagnetic phase the corresponding graph will again have two peaks, but now these will be much narrower and higher, approaching two Dirac deltas in the thermodynamic limit. Suppose we want to perform the double limit of Eq. (67). This would involve introducing a small magnetic field which would shift the origin of $\hat{h}$ (29). The neighbourhood of one of the peaks would then become exponentially suppressed and eventually disappear in the thermodynamic limit. Thus, we can mimic the effect of Eq. (67) by considering only one of the two peaks from the beginning. This would not work below $\beta_c$, as there the peaks extrapolate to $m = 0$ (recall Section 5.3). In a more complex model, the $L$ evolution of the right peak should be checked, in order not to mistake a paramagnetic phase for a ferromagnetic one. This criterion suggests that TMC could be a powerful method for determining the order of magnetic phase transitions.

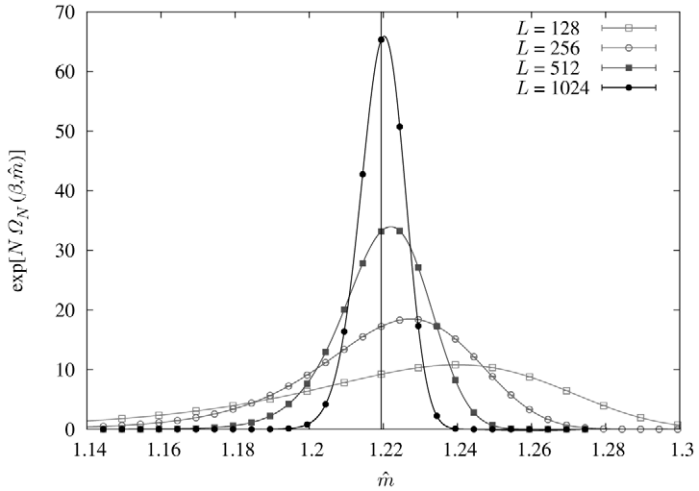


Fig. 7. Computation at $\beta = 0.4473 > \beta_c$ (ferromagnetic phase). The peak of the pdf of $\hat{m}$ gets narrower and closer to $m_Y + 1/2$ as $L$ increases (the vertical line, where $m_Y$ is Yang's magnetisation for the infinite system at $\beta = 0.4473$ [43]). Compare the scale of the $x$ axis and the height of the peaks with those of Fig. 1.

This procedure has the considerable advantage that it works for any lattice size. In this section we have chosen the peak of positive magnetisation. We will illustrate it by considering the thermodynamic limit in the canonical ensemble in Section 8.1 and by studying the equivalence between the tethered and canonical ensembles in Section 8.2.

### *8.1. The thermodynamic limit*

We have run simulations for lattice sizes $L = 128, 256, 512, 1024$ at $\beta = 0.4473 > \beta_c$. This temperature was chosen because we estimated that it would roughly mirror the value of the correlation length[7] for our paramagnetic simulations.

Following the previous discussion, we have worked in the $\hat{m} > 0.5$ (positive magnetisation) region, where there is only one peak. An appropriate sampling of $\hat{m}$ is even more important in this phase (but easier to optimise) than in the situation described in detail in Section 3.1. The reason is that the peak is now so narrow that a choice of $\hat{m}$ spaced as in the aforementioned section would not only be completely wasteful, but may also completely fail to sample the peak.

In the case of the Ising model, we know Yang's exact solution $m_Y(\beta)$ for the magnetisation of the infinite system [43]. The positive peak for $p(\hat{m})$ will then be very close to $m_Y(\beta) + \frac{1}{2}$ and get closer as we increase $L$. With this information in hand, we can adequately reconstruct the effective potential by running simulations in a small neighbourhood of $m_Y(\beta) + \frac{1}{2}$. For a different model, where we would lack the knowledge of the peak's position in the thermodynamic limit, we can just run simulations with a very fine grid for some small and essentially costless lattice size and infer from them an efficient distribution of points for the larger systems.

We have represented $p(\hat{m})$ for all the simulated lattices in Fig. 7, which includes the whole range of $\hat{m}$ for $L \geqslant 512$ (for the smaller lattices we have used a somewhat larger interval). It is interesting to compare the scale on the $x$ axis with that of Fig. 1. As will be discussed in detail in

[7] In the ferromagnetic regime $\xi_1$ is not a good definition and we always use $\xi_2$, see Eq. (13).

Table 7
Canonical averages for several physical quantities of an Ising lattice at $\beta = 0.4473$ computed with the tethered method (T). The grid of $\hat{m}$ values is uniform in the narrow simulated band. Also included are the exact results for finite lattices from [26] and the exact results in the thermodynamic limit from [12,43]. We appreciate that by simulating only a very small range $\Delta\hat{m}$ of values for $\hat{m}$ we can obtain very precise values. Within our error, we have already reached the thermodynamic limit for $L = 512$

| $L$ | $N_{\text{points}}$ | $\Delta\hat{m}$ | $-\langle u\rangle_\beta$ | $C$ | $\xi_2$ | $\langle m^2\rangle_\beta$ | $\langle m\rangle_\beta$ | $\chi_2$ |
|---|---|---|---|---|---|---|---|---|
| 128 (T) | 90 | 0.9 | 1.490397(18) | 8.874(4) | 10.394(17) | 0.51987(8) | 0.71934(6) | 39.65(8) |
| 128 (E) | | | 1.490409763... | 8.877363... | | | | |
| 256 (T) | 79 | 0.39 | 1.490407(11) | 8.869(5) | 11.26(4) | 0.51816(5) | 0.71941(4) | 39.36(7) |
| 256 (E) | | | 1.490415672... | 8.874075... | | | | |
| 512 (T) | 27 | 0.13 | 1.490419(5) | 8.877(5) | 11.5(3) | 0.51777(4) | 0.71945(3) | 39.37(9) |
| 512 (E) | | | 1.490415689... | 8.874046... | | | | |
| 1024 (T) | 27 | 0.13 | 1.490416(4) | 8.868(7) | 11.4(18) | 0.51764(4) | 0.71945(2) | 39.48(11) |
| 1024 (E) | | | 1.490415689... | 8.874046... | | | | |
| $\infty$ (E) | | | 1.490415689... | 8.874046... | | | 0.719436... | |

Section 8.2, the peak approaches $m_{\text{Y}}(\beta) + \frac{1}{2}$ (the vertical line) as $L$ increases. Table 7 compares the values of the energy and specific heat obtained in our simulations with the exact values given in [26]. Notice how very small simulated ranges of $\hat{m}$ ($\Delta\hat{m} = \hat{m}_{\max} - \hat{m}_{\min}$) yield very accurate results. In fact, we can see that for the $L = 1024$ lattice we obtain a more precise determination for the energy with 27 points than what we obtained at the critical temperature with 77 (we still perform $10^7$ Monte Carlo sweeps in each point). This result is even more impressive if we consider that some of these 27 points, being deeply inside the tails of the distribution, do not have any effect whatsoever in the average with our error (of course, we do not know this until we have run the simulation and seen the actual width of the peak).

From Table 7 we can conclude that the thermodynamic limit has already been reached for $L = 256$, at least to the level indicated by our errors. Our whole computation for $L = 512$ required about 270 hours of computer time. For comparison, a 30 hour long Swendsen–Wang computation of the correlation length for $L = 512$ gives $\xi_2 = 11.8(2)$. We see that the ratio of computation time for both methods has changed significantly from the critical point, where the advantage of the cluster algorithm was much greater.

Let us now consider the curve for $m_\beta(h) = \langle m\rangle_\beta(h)$ in the thermodynamic limit. We compute it with the same method employed in Section 7, but now we cannot apply the antisymmetrisation (59). The result is plotted in Fig. 8, where we plot $L = 512$ for magnetic fields in the range $h \in [0, 10^{-3}]$. We also plot $L = 256$ to check that both curves coincide and we have reached the thermodynamic limit within our errors. We appreciate in this figure just how efficient the antisymmetrisation procedure was in Fig. 5, which had much smaller errors.

### 8.2. *Ensemble equivalence in the ferromagnetic phase*

Once we wander away from the critical point, the main objective is finding the value of physical quantities in the thermodynamic limit. The ensemble equivalence property suggests a way to reach this limit without constructing the whole canonical $p(\hat{m})$, but by concentrating instead on its maximum. From the computational point of view, this supposes a dramatic reduction in the needed effort for a TMC simulation.

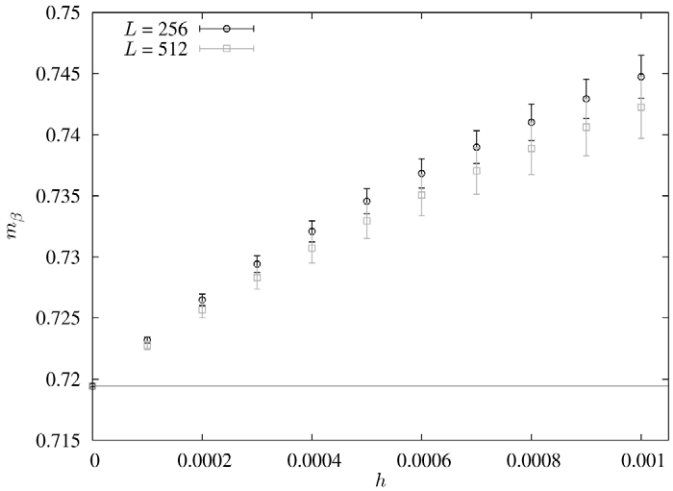


Fig. 8. Magnetisation in the presence of a magnetic field in the ferromagnetic regime for $\beta = 0.4473$. The horizontal line is the exactly known thermodynamic limit for $h = 0$.

Ensemble equivalence can be expressed in mathematical terms by

$$\lim_{N\to\infty} \langle O\rangle_\beta = \lim_{N\to\infty} \langle O\rangle_{\langle \hat{m}\rangle_\beta,\beta}. \tag{68}$$

This equation can be understood as a more formal way of summarising the behaviour of Fig. 7. Indeed, we saw in the previous section that we could reconstruct the canonical averages considering only a very narrow range of $\hat{m}$; in the thermodynamic limit a single point would be sufficient.

For the Ising model we can situate this point exactly because we know Yang's spontaneous magnetisation

$$\hat{m}_{\mathrm{Y}}(\beta) = \lim_{N\to\infty} \langle \hat{m}\rangle_\beta = \lim_{N\to\infty} \langle m\rangle_\beta + \frac{1}{2} = \left[1 - (\sinh 2\beta)^{-4}\right]^{1/8} + \frac{1}{2}. \tag{69}$$

We could then run simulations for several lattice sizes at precisely $\hat{m}_{\mathrm{Y}}$ and study the evolution of $\langle O\rangle_{\hat{m}_{\mathrm{Y}},\beta}$ as we increase $L$. This is not the most practical approach, as for a model other than the $D = 2$ Ising lattice we would not know the position of the peak beforehand. Instead, we will follow a more general analysis that would work in more complex situations.

Let us consider the canonical average of some quantity and recall that we are using periodic boundary conditions, so the approach to the thermodynamic limit is exponential

$$\langle O\rangle_\beta = \int_{1/2}^{\infty} \mathrm{d}\hat{m}\, p(\hat{m},\beta;L)\langle O\rangle_{\hat{m}} = O_\beta^\infty + A_O \mathrm{e}^{-L/\xi_\infty}, \tag{70}$$

where $A_O$ is a constant amplitude. We have just considered the positive magnetisation peak.

Since the integral will be dominated by a saddle point at $\hat{m}^+_{\mathrm{peak}}$, with $\hat{m}^+_{\mathrm{peak}} \overset{L\to\infty}{\longrightarrow} \hat{m}_{\mathrm{Y}}$, we can approximate the pdf by a Gaussian

$$p(\hat{m},\beta;L) \simeq \sqrt{\frac{N}{2\pi\chi_2}} \exp\left[-\frac{N(\hat{m}-\hat{m}_{\mathrm{peak}})^2}{2\chi_2}\right]. \tag{71}$$

Table 8
Tethered mean values of several parameters at the peak of the probability density function for $\beta = 0.4473$ and $\beta = 0.6$, together with the value of $\hat{h}_{\mathrm{Y}} = \langle \hat{h} \rangle_{\hat{m}_{\mathrm{Y}}}$ (this observable is zero at the peak and helps characterise how close we are to it). The exact value for an infinite lattice, which coincides with the canonical average, is also included for comparison

| $L$ | $\beta = 0.4473$ | | | $\beta = 0.6$ | | |
|---|---|---|---|---|---|---|
| | $\hat{h}_{\mathrm{Y}} \times 10^5$ | $\hat{m}^+_{\mathrm{peak}}$ | $-u^+_{\mathrm{peak},\beta}$ | $\hat{h}_{\mathrm{Y}} \times 10^5$ | $\hat{m}^+_{\mathrm{peak}}$ | $-u^+_{\mathrm{peak},\beta}$ |
| 16 | 2984(3) | 1.34384(4) | 1.57707(8) | −290.6(14) | 1.471 943(7) | 1.91298(4) |
| 32 | 924.7(16) | 1.29930(7) | 1.52898(9) | −52.5(8) | 1.473 299(5) | 1.91018(2) |
| 64 | 284.9(9) | 1.26333(7) | 1.50548(5) | −11.0(4) | 1.473 543(2) | 1.909374(9) |
| 128 | 86.0(6) | 1.23988(9) | 1.49563(4) | −2.45(19) | 1.473 5940(12) | 1.909165(5) |
| 256 | 25.5(3) | 1.22732(8) | 1.49199(2) | −0.67(11) | 1.473 6047(2) | 1.909107(3) |
| 512 | 6.9(2) | 1.22204(6) | 1.490859(16) | −0.19(5) | 1.473 6077(4) | 1.9090907(15) |
| 1024 | 2.11(11) | 1.22024(4) | 1.490538(9) | −0.03(2) | 1.473 6083(2) | 1.9090867(4) |
| $\infty$ | 0 | 1.219435... | 1.490416... | 0 | 1.4736087... | 1.9090862... |

Therefore, we expect the tethered average of $O$ at this saddle point to approach the canonical average (70), with a correction of order $N^{-1}$,

$$O^{\infty}_{\beta} = \langle O \rangle_{\beta} - A_O \mathrm{e}^{-L/\xi_{\infty}} = \langle O \rangle_{\hat{m}^+_{\mathrm{peak}},\beta} + \mathcal{O}\big(L^{-D}\big). \tag{72}$$

To ease the notation we shall use the definition

$$O^+_{\mathrm{peak},\beta} = \langle O \rangle_{\hat{m}^+_{\mathrm{peak}},\beta}. \tag{73}$$

This simple analysis provides a practical way of approaching the thermodynamic limit without knowing the limiting position of the peak in advance.

We first run a complete simulation for some small lattice, covering the whole range of $\hat{m}$. This provides a first approximation to the position of the peak. For growing lattices, we just compute two or three points at both sides of where we think the maximum is going to be. Our objective is not to reconstruct the whole peak of $p(\hat{m})$, just to find a good approximation to the point $\hat{m}^+_{\mathrm{peak}}$ where $\langle \hat{h} \rangle_{\hat{m},\beta}$ vanishes. We use the same procedure as in Section 5.3, finding the zero of the cubic spline and interpolating the physical observables. Actually, if the position of the peak is sufficiently bounded we could just place one point very closely at either side and use a linear interpolation.

With this procedure we are able to compute the tethered mean values of the relevant physical quantities at the peak with a minimum of numerical effort. Here we shall apply this method to the energy and we shall also characterise the approach of the peak to $\hat{m}_{\mathrm{Y}}$. To the latter purpose, we have computed $h_{\mathrm{Y}} = \langle \hat{h} \rangle_{\hat{m}_y,\beta}$ for several lattice sizes and studied how fast it approaches zero. We also give the values for the position of the peak (Table 8).

Following the above analysis we should find that

$$\begin{aligned} \big|u^+_{\mathrm{peak},\beta} - u^{\infty}_{\beta}\big| &= A_u \cdot L^{-\zeta_u}, \\ \big|\hat{m}^+_{\mathrm{peak},\beta} - \hat{m}_{\mathrm{Y}}\big| &= A_{\hat{m}} \cdot L^{-\zeta_{\hat{m}}}, \\ \hat{h}_{\mathrm{Y}} &= A_{\hat{h}} \cdot L^{-\zeta_{\hat{h}}}, \end{aligned} \tag{74}$$

with $\zeta \approx 2$. We have tried to fit these quantities to a power law for $\beta = 0.4473$, but we found its behaviour to be more complex. Instead, we present in Table 9 the result of taking the points for $L$ and $2L$ and computing the effective exponent between them (that is, the value of $\zeta$ so that the

Table 9
Rate at which several observables approach zero. We consider a functional form $A \cdot L^{-\zeta}$ and compute the effective exponent $\zeta$ from the ratio of the computed values at consecutive lattice sizes. We consider three exponents, $\zeta_{\hat{h}}$, $\zeta_{\hat{m}}$ and $\zeta_u$ for the evolution of $\hat{h}_{\rm Y}$, $\hat{m}^+_{\rm peak}$ and $u^+_{\rm peak}$, respectively, see Eq. (74). We observe that for $\beta = 0.6$ the effective exponent approaches 2, as expected from the discussion in the text, while for $\beta = 0.4473$ the proximity of the critical point complicates the analysis

| $L$ | $\beta = 0.4473$ | | | $\beta = 0.6$ | | |
|---|---|---|---|---|---|---|
| | $\zeta_{\hat{h}}$ | $\zeta_{\hat{m}}$ | $\zeta_u$ | $\zeta_{\hat{h}}$ | $\zeta_{\hat{m}}$ | $\zeta_u$ |
| 16 | 1.690(3) | 0.6394(14) | 1.168(4) | 2.47(2) | 2.43(2) | 1.83(3) |
| 32 | 1.699(5) | 0.864(3) | 1.356(6) | 2.25(5) | 2.24(5) | 1.93(5) |
| 64 | 1.729(12) | 1.102(7) | 1.531(12) | 2.17(12) | 2.16(13) | 1.87(10) |
| 128 | 1.75(2) | 1.375(16) | 1.73(3) | 1.9(3) | 1.89(13) | 1.9(2) |
| 256 | 1.88(5) | 1.60(4) | 1.83(6) | 1.8(4) | 2.0(5) | 2.2(5) |
| 512 | 1.71(9) | 1.70(8) | 1.85(12) | 2.7(12) | 1.4(10) | 3.1(12) |

power law would pass exactly by those points). As we can see, our results are always $\zeta < 2$, even though this exponent grows with $L$.

We believe this was caused by the proximity of the critical point, so we ran analogous simulations for $\beta = 0.6$. We were able to complete this new computations in very little time, following the above procedure. For example, for $L = 512$ the position of the peak was so well bounded that we just computed one point at either side.

Comparing Table 8 with Table 2 we see that for $\beta = 0.6$, with a computation effort almost 40 times smaller, we have obtained a result an order of magnitude more precise than what we had at $\beta_{\rm c}$. Recomputing the effective exponents for these new simulations we obtain results compatible with $\zeta = 2$. Notice that for this temperature the error in the exponents is much bigger than that for $\beta = 0.4473$. The reason is clear from Table 8. The left-hand sides of Eqs. (74) are now much closer to zero than in $\beta = 0.4473$, yet their errors are only slightly smaller. In the computation of the effective exponents only the relative errors matter, which explains our bigger uncertainties. Notice, however, that we have been able to distinguish values for $h_{\rm Y}$ of order $10^{-6}$ from zero and that we have located the peak with seven significant figures.

## 9. Conclusions and outlook

We have presented the Tethered Monte Carlo method, a completely unspecific formalism to reconstruct the effective potential of the order parameter. This method is based on a new statistical ensemble, which we have described in detail. The tethered ensemble not only allows us to reproduce the canonical results, but is also specially suited to the study of the broken symmetry phase and the effects of an external magnetic field.

We have implemented this formalism in the $D = 2$ Ising model, were we can make exhaustive checks of our results, either against exact solutions or high precision computations performed with canonical cluster algorithms. We have not have tried to optimise the efficiency for this particular model, choosing instead the most generally appliable method: a standard local Metropolis algorithm. The possibility of developing a cluster algorithm for the tethered formalism will be considered in the future.

The method has been tested to a high degree of accuracy in a large variety of situations: the critical point, the scaling paramagnetic region, the thermodynamic limit in the ferromagnetic region and the nonlinear response to an external magnetic fields. Our Monte Carlo implementation

has proven to be remarkably efficient for the ferromagnetic phase and specially for computations with an external magnetic field.

One of its most conspicuous features is the absence of critical slowing down for all functions of the magnetisation, even though we have used a local algorithm. This is probably due to the fact that the tethered ensemble instantaneously propagates information to the whole lattice by means of a 'magnetic bath'. Our algorithm allows us to study each magnetisation independently without having to wander randomly in the magnetisation space, as is the case for multicanonical or Wang–Landau computations.

We expect Tethered Monte Carlo to be of great help whenever large tunnelling barriers appear, associated to observables not present in the Hamiltonian. A non-exhaustive list of instances are the standard magnetisation in the Random Field Ising Model [44], the staggered magnetisation for the Diluted Antiferromagnet in a Field [45] or the Polyakov loop for lattice gauge theories [8]. In these cases 'tethering' extensive quantities other than the magnetisation could prove an invaluable guide for the exploration of phase space. In particular, we wish to apply this formalism in the near future to undertake a thorough study of the condensation transition [21,46].

## Acknowledgements

We were partially supported by MEC (Spain) through contract No. FIS-2006-08533-C03-01 and by CAM (Spain) through contract No. CCG07-UCM/ESP-2532.

## Appendix A. Some numerical details

A numerical implementation of Eq. (28) can be done in several different ways of equivalent numerical accuracy. Here we briefly explain our choices.

Recall that we have represented $\langle \hat{h} \rangle_{\hat{m},\beta}$ with a cubic spline interpolation. We have not used the so-called natural spline, which imposes vanishing curvature for $\langle \hat{h} \rangle_{\hat{m},\beta}$ at $\hat{m}_{\max}$ and $\hat{m}_{\min}$. Instead, we have estimated the derivative of this function at both ending points with a parabolic interpolation. To compute the canonical average of (28) we also represent $\langle O \rangle_{\hat{m},\beta}$ with a cubic spline. However, naively applying this interpolation scheme for the exponential, $p(\hat{m}) = \exp[N\Omega_N(\hat{m})]$, could introduce strong integration errors. Fortunately, this can be easily solved by accurately representing the exponent $N\Omega_N$, which is a smooth function (recall the curve in logarithmic scale of Fig. 1).

$\Omega_N(\hat{m}, \beta)$, being the integral of the cubic spline for $\langle \hat{h} \rangle_{\hat{m},\beta}$, is a fourth order polynomial between each pair of consecutive points in the $\hat{m}$ grid, which can be exactly computed from the coefficients of the cubic spline. To avoid losing precision, we evaluate $\Omega_N(\hat{m}, \beta)$ at an extended grid that includes 3 equally spaced intermediate points between each pair of simulated values of $\hat{m}$. This way the Lagrange interpolating polynomial for each segment of the extended lattice (two original points plus three intermediate ones) represents the exact integral of our spline.

Of course, the pdf, $\exp[N\Omega_N(\hat{m}, \beta)]$, is not a polynomial anymore. It is, however, a smooth function so a self consistent Romberg method [31] provides an estimate of the integral (28) with any required numerical accuracy. Notice that this yields the basically exact results for a given interpolation of $\langle \hat{h} \rangle_{\hat{m},\beta}$, but it does not cure any discretisation errors introduced by the spline.

Typically, even with a very moderate effort, the Romberg integration error has been much smaller than the statistical one. There is one exception: the fluctuation–dissipation formulas, such as (7), because of the large cancellations between the two terms. To solve this problem, we

have computed the fluctuation–dissipation formula as a sum of two squares:

$$N^{-1}C = \langle u^2\rangle_\beta - \langle u\rangle_\beta^2 = \int \mathrm{d}\hat{m}\; p(\hat{m})\big[\langle u^2\rangle_{\hat{m}} - \langle u\rangle_{\hat{m}}^2 + \langle u\rangle_{\hat{m}}^2 - \langle u\rangle_\beta^2\big]$$
$$= \int \mathrm{d}\hat{m}\; p(\hat{m})\big[\big\langle\big(u - \langle u\rangle_{\hat{m}}\big)^2\big\rangle_{\hat{m}} + \big(\langle u\rangle_{\hat{m}} - \langle u\rangle_\beta\big)^2\big]. \tag{A.1}$$

In spite of this, as a consistency check, we have also employed the original equation and forced the Romberg integral to yield the same value, by reducing its tolerance.

## References


[1] D.J. Amit, V. Martin-Mayor, Field Theory, the Renormalization Group and Critical Phenomena, third ed., World Scientific, Singapore, 2005.
[2] J. Zinn-Justin, Quantum Field Theory and Critical Phenomena, third ed., Clarendon Press, Oxford, 1996.
[3] A. Pelissetto, E. Vicari, Phys. Rep. 368 (2002) 549.
[4] D.P. Landau, K. Binder, A Guide to Monte Carlo Simulations in Statistical Physics, second ed., Cambridge Univ. Press, 2005;
M.E.J. Newman, G.T. Barkema, Monte Carlo Methods in Statistical Physics, Clarendon Press, Oxford, 1999.
[5] A.D. Sokal, in: C. DeWitt-Morette, P. Cartier, A. Folacci (Eds.), Functional Integration: Basics and Applications, 1996 Cargèse school, Plenum, New York, 1997.
[6] R.H. Swendsen, J.-S. Wang, Phys. Rev. Lett. 58 (1987) 86;
U. Wolff, Phys. Rev. Lett. 62 (1989) 361.
[7] Y. Deng, T.M. Garoni, W. Guo, H.W.J. Blöte, A.D. Sokal, Phys. Rev. Lett. 98 (2007) 120601;
Y. Deng, T.M. Garoni, A.D. Sokal, Phys. Rev. Lett. 99 (2007) 110601;
Y. Deng, T.M. Garoni, A.D. Sokal, cond-mat/0701113;
Y. Deng, T.M. Garoni, J. Machta, G. Ossola, M. Polin, A.D. Sokal, arXiv: 0705.2751.
[8] H.J. Rothe, Lattice Gauge Theories: An Introduction, third ed., World Scientific, Singapore, 2005;
M. Creutz, Quarks, Gluons and Lattices, Cambridge Univ. Press, 1985.
[9] See, e.g., P.G. Benedetti, Metastable Liquids, Princeton Univ. Press, 1997.
[10] See, e.g., M. Mezard, G. Parisi, M. Virasoro, Spin-Glass Theory and Beyond, World Scientific, Singapore, 1987;
J.A. Mydosh, Spin Glasses: An Experimental Introduction, Taylor and Francis, London, 1993.
[11] J.N. Onuchic, Z. Luthey-Schulten, P.G. Wolynes, Annu. Rev. Phys. Chem. 48 (1997) 545.
[12] L. Onsager, Phys. Rev. 65 (1944) 117.
[13] A.B. Zamolodchikov, Adv. Stud. Pure Math. 19 (1989) 641;
A.B. Zamolodchikov, Int. J. Mod. Phys. A 4 (1989) 4235.
[14] G. Delfino, G. Mussardo, P. Simonetti, Nucl. Phys. B 473 (1996) 469;
P. Fonseca, A. Zamolodchikov, J. Stat. Phys. 110 (2003) 527;
See G. Delfino, J. Phys. A 37 (2004) R45, for a review.
[15] M. Caselle, P. Grinza, N. Magnoli, Nucl. Phys. B 579 (2000) 635;
P. Grinza, A. Rago, Nucl. Phys. B 651 (2003) 387;
M. Caselle, P. Grinza, A. Rago, J. Stat. Mech. 0410 (2004) P009.
[16] N. Metropolis, A.W. Rosenbluth, N.M. Rosenbluth, A.H. Teller, E. Teller, J. Chem. Phys. 21 (1953) 1087.
[17] V. Martin-Mayor, Phys. Rev. Lett. 98 (2007) 137207.
[18] L.A. Fernandez, A. Gordillo-Guerrero, V. Martin-Mayor, J.J. Ruiz-Lorenzo, Phys. Rev. Lett. 100 (2008) 057201.
[19] M. Creutz, Phys. Rev. Lett. 50 (1983) 1411.
[20] B.A. Berg, T. Neuhaus, Phys. Rev. Lett. 68 (1992) 9.
[21] A. Nußbaumer, E. Bittner, T. Neuhaus, W. Janke, Europhys. Lett. 75 (2006) 716;
A. Nußbaumer, E. Bittner, W. Janke, Phys. Rev. E 77 (2008) 041109.
[22] F. Wang, D.P. Landau, Phys. Rev. Lett. 86 (2001) 2050.
[23] C. Zhou, T.C. Schulthess, S. Torbrügge, D.P. Landau, Phys. Rev. Lett. 96 (2006) 120201;
S.-H. Tsai, F. Wang, D.P. Landau, Phys. Rev. E 75 (2007) 061108.
[24] K. Kawasaki, Phys. Rev. 145 (1966) 224.
[25] B.M. McCoy, T.T. Wu, The Two Dimensional Ising Model, Harvard Univ. Press, 1973.
[26] A.E. Ferdinand, M.E. Fisher, Phys. Rev. 185 (1969) 832.

[27] F. Cooper, B. Freedman, D. Preston, Nucl. Phys. B 210 (1982) 210.
[28] S. Caracciolo, R.G. Edwards, S.J. Ferreira, A. Pelissetto, A.D. Sokal, Phys. Rev. Lett. 74 (1995) 2969.
[29] H.G. Ballesteros, L.A. Fernandez, V. Martin-Mayor, A. Muñoz Sudupe, Phys. Lett. B 378 (1996) 207;
H.G. Ballesteros, L.A. Fernandez, V. Martin-Mayor, A. Muñoz Sudupe, Nucl. Phys. B 483 (1997) 707.
[30] F. Belletti, et al., JANUS Collaboration, Comput. Sci. Eng. 8 (2006) 41;
F. Belletti, et al., JANUS Collaboration, Comput. Phys. Commun. 178 (2008) 208, arXiv: 0710.3535.
[31] W.H. Press, S.A. Teukolsky, W.T. Vetterling, B.P. Flannery, Numerical Recipes in C, second ed., Cambridge Univ. Press, 1992.
[32] G. Ossola, A.D. Sokal, Nucl. Phys. B 691 (2004) 259.
[33] G. Ossola, A.D. Sokal, Phys. Rev. E 70 (2004) 027701.
[34] G. Parisi, F. Rapuano, Phys. Lett. B 157 (1985) 301.
[35] P.C. Hohenberg, B. Halperin, Rev. Mod. Phys. 49 (1977) 435.
[36] P. Tamayo, W. Klein, Phys. Rev. Lett. 63 (1989) 2757.
[37] J. Salas, A.D. Sokal, J. Stat. Phys. 98 (2000) 551.
[38] H.G. Ballesteros, L.A. Fernandez, A. Muñoz Sudupe, V. Martin-Mayor, Phys. Lett. B 387 (1996) 125.
[39] M. Caselle, M. Hasenbusch, A. Pelissetto, E. Vicari, J. Phys. A: Math. Gen. 34 (2001) 2923.
[40] J. Balog, M. Niedermaier, F. Niedermayer, A. Patrascioiu, E. Seiler, P. Weisz, Nucl. Phys. B 583 (2000) 614.
[41] J.-K. Kim, J. Phys. A: Math. Gen. 33 (2000) 2675.
[42] M. Sweeny, Phys. Rev. B 27 (1983) 4445;
U. Wolff, Nucl. Phys. B 300 (1988) 501.
[43] C.N. Yang, Phys. Rev. 85 (1952) 808.
[44] T. Natterman, in: A.P. Young (Ed.), Spin Glasses and Random Fields, World Scientific, Singapore, 1997.
[45] A. Maiorano, V. Martin-Mayor, J.J. Ruiz-Lorenzo, A. Tarancon, Phys. Rev. B 76 (2007) 064435.
[46] M. Biskup, L. Chayes, R. Kotecký, Europhys. Lett. 60 (2002) 21;
K. Binder, Physica (Amsterdam) 319A (2003) 99;
L.G. MacDowell, P. Virnau, M. Müller, K. Binder, J. Chem. Phys. 120 (2004) 5293.